Hsp40s play distinct roles during the initial stages of apolipoprotein B biogenesis

Deepa Kumari[a], Edward A. Fisher[b], and Jeffrey L. Brodsky[a,*]
[a]Department of Biological Sciences, University of Pittsburgh, Pittsburgh, PA 15260; [b]Department of Medicine, Leon H. Charney Division of Cardiology, Cardiovascular Research Center, New York University Grossman School of Medicine, New York, NY 10016

ABSTRACT **Apolipoprotein B (ApoB) is the primary component of atherogenic lipoproteins, which transport serum fats and cholesterol. Therefore elevated levels of circulating ApoB are a primary risk factor for cardiovascular disease. During ApoB biosynthesis in the liver and small intestine under nutrient-rich conditions, ApoB cotranslationally translocates into the endoplasmic reticulum (ER) and is lipidated and ultimately secreted. Under lipid-poor conditions, ApoB is targeted for ER-associated degradation (ERAD). Although prior work identified select chaperones that regulate ApoB biogenesis, the contributions of cytoplasmic Hsp40s are undefined. To this end, we screened ApoB-expressing yeast and determined that a class A ER-associated Hsp40, Ydj1, associates with and facilitates the ERAD of ApoB. Consistent with these results, a homologous Hsp40, DNAJA1, functioned similarly in rat hepatoma cells. DNAJA1-deficient cells also secreted hyperlipidated lipoproteins in accordance with attenuated ERAD. In contrast to the role of DNAJA1 during ERAD, DNAJB1—a class B Hsp40—helped stabilize ApoB. Depletion of DNAJA1 and DNAJB1 also led to opposing effects on ApoB ubiquitination. These data represent the first example in which different Hsp40s exhibit disparate effects during regulated protein biogenesis in the ER and highlight distinct roles that chaperones can play on a single ERAD substrate.**

Monitoring Editor
Elizabeth Miller
MRC Laboratory of Molecular Biology

Received: Sep 13, 2021
Revised: Nov 29, 2021
Accepted: Dec 6, 2021

INTRODUCTION

Each year, cardiovascular disease kills ~18 million people, and one in four deaths in the United States is due to cardiovascular disease (Heron, 2017; Benjamin *et al.*, 2019). Coronary artery disease (CAD) is the most common form of cardiovascular disease and arises when arteries narrow due to the deposition of cholesterol-filled macrophages that form plaques. This process, known as atherosclerosis, can lead to angina from lumenal narrowing or to a heart attack if a plaque ruptures and causes an acute thrombotic occlusion. Current treatments for CAD include drugs that target various aspects of lipid metabolism, including the synthesis, transport, and endocytosis of lipids and/or cholesterol (Goldstein and Brown, 2015; Adhyaru and Jacobson, 2018; Larsen *et al.*, 2019; Libby and Everett, 2019). The most commonly used drugs are the statins. For the vast majority of individuals, statins represent an effective first-line treatment to lower the risk of CAD, but the response to statins varies widely. For example, the decrease in circulating levels of low-density lipoproteins (LDLs) can vary from 5–70% in an individual (Reiner *et al.*, 2013; Reiner and Tedeschi-Reiner, 2013). This variation most often arises from polymorphisms in genes linked to statin metabolism (i.e., pharmacodynamics and pharmacokinetics) (Reiner, 2014; Sikka *et al.*, 2011; Dadu and Ballantyne, 2014; Ward *et al.*, 2019). Moreover, in some patients, statins elicit several side effects including muscle weakness, leg cramps, and myopathy, forcing select individuals to discontinue medication or to lower the dose. Therefore it is imperative to identify new therapeutic targets to combat CAD.

This article was published online ahead of print in MBoC in Press (http://www.molbiolcell.org/cgi/doi/10.1091/mbc.E21-09-0436) on December 15, 2021.

*Address correspondences to: Jeffrey L. Brodsky (jbrodsky@pitt.edu).

Abbreviations used: ApoB, Apolipoprotein B; ApoB100, full-length apolipoprotein B; ApoB48, N-terminal 48% of the apolipoprotein B polypeptide; CAD, coronary artery disease; CFTR, cystic fibrosis transmembrane conductance regulator; CTD, C-terminal domain; DDM, dodecyl maltoside; DPBS, Dulbecco phosphate-buffered saline; DSP, dithiobis(succinimidyl propionate); ER, endoplasmic reticulum; ERAD, endoplasmic reticulum-associated degradation; FBS, fetal bovine serum; HDL, high-density lipoprotein; Hsp, heat shock protein; IF, indirect immunofluorescence; JDP, J domain protein; LDL, low-density lipoprotein; MTP, microsomal triglyceride transfer protein; PDI, protein disulfide isomerase; PMSF, phenylmethylsulfonyl fluoride; TCA, trichloroacetic acid; VLDL, very low-density lipoprotein; YPD, yeast peptone dextrose; ZFLR, zinc fingerlike region.

Triacylglycerol, phospholipids, cholesterol, and cholesterol esters are transported through the circulatory system in lipoprotein particles. The major structural component of these atherogenic very low-density lipoproteins (VLDLs), LDLs, and chylomicrons is apolipoprotein B (ApoB), a ~550 kDa amphipathic protein (Bostrom *et al.*, 1986; Olofsson *et al.*, 1987; Boren *et al.*, 1994). (In contrast, high-density lipoproteins [HDLs] are ApoAI and ApoAII associated.) ApoB aids in the assembly, secretion, transport, and cellular uptake of lipoproteins. In mammals, ApoB is expressed in the liver and small intestine in two different isoforms, ApoB100 and ApoB48, which represent the full-length and N-terminal 48% portion of the full-length protein, respectively (Chen *et al.*, 1986, 1987, 1988; Powell *et al.*, 1987; Hussain *et al.*, 1996, 2005). Not surprisingly, there is a direct correlation between circulating ApoB and CAD: higher levels cause CAD, whereas lower levels are associated with normal homeostasis or, if severely limited, with hypobetalipoproteinemia, which presents as delayed development, hepatomegaly, steatorrhea, and cytolysis (Jang *et al.*, 2020; Welty, 2020). Based on its central role in lipoprotein metabolism, ApoB has been directly targeted to treat CAD (Zimmermann *et al.*, 2006; Boekholdt *et al.*, 2014; Reyes-Soffer *et al.*, 2016; Nandakumar *et al.*, 2018). Unfortunately, a second generation ApoB-targeted antisense oligonucleotide-based drug (Mipomersen) is effective yet exhibits severe side effects (namely, liver damage) (Astaneh *et al.*, 2021). Nevertheless, these data position ApoB as a bona fide therapeutic target.

As nascent ApoB is cotranslationally translocated into the endoplasmic reticulum (ER) through the Sec61 translocon, the apolipoprotein is lipidated by the ER lumenal microsomal triglyceride transfer protein (MTP) complex and a premature lipoprotein particle is formed (Wu *et al.*, 1996; Fisher *et al.*, 1997; Mitchell *et al.*, 1998; Zhou *et al.*, 1998). This pre-VLDL particle then exits the ER via a nonclassical pathway that requires enlarged COPII vesicles. The particle next enters the Golgi where it undergoes further lipidation and lipid remodeling before it is finally secreted (Gusarova *et al.*, 2003; Siddiqi *et al.*, 2003; Butkinaree *et al.*, 2014; Sane *et al.*, 2017). In contrast, if a cell lacks adequate lipids—or in the absence of MTP function—ER entry is slowed so continued translation exposes hydrophobic ApoB loops in the cytosol (Gordon *et al.*, 1996). These potentially aggregation-prone loops are recognized by molecular chaperones, which in theory could help maintain solubility and facilitate ubiquitination by an ER resident E3 ubiquitin ligase, gp78 (Liang *et al.*, 2003b; Fisher *et al.*, 2011). Ultimately, ApoB is degraded by the cytosolic 26S proteasome with the aid of the AAA^+-ATPase p97/VCP (Fisher *et al.*, 1997, 2008; Rutledge *et al.*, 2009). Over many years, our group and others have identified and characterized several classes of molecular chaperones, including BiP, heat shock protein (Hsp)70, Hsp90, Hsp110, Hsp104, protein disulfide isomerase (PDI), calnexin, and calreticulin, which play various roles during the folding and ER-associated degradation (ERAD) of ApoB (Zhou *et al.*, 1995; Fisher *et al.*, 1997; Ginsberg, 1997; Chen *et al.*, 1998; Tatu and Helenius, 1999; Gusarova *et al.*, 2001; Hrizo *et al.*, 2007; Rutledge *et al.*, 2013; Doonan *et al.*, 2019).

Although Hsp70 is one of the many chaperones that regulate ApoB biogenesis, the function of this chaperone commonly requires an Hsp40 partner. Hsp40s, also known as J domain proteins (JDPs), are present in all cell types and assist Hsp70s by enhancing Hsp70 ATPase activity and facilitating substrate targeting and selectivity (Kampinga and Craig, 2010; Craig and Marszalek, 2017). Like Hsp70s, Hsp40s also play essential roles during protein folding, assembly, translocation, the prevention of aggregation, ubiquitination, and degradation (Kampinga *et al.*, 2019). In addition, Hsp40s reside in one of three classes, which are based on sequence similarity and domain architecture. Recent work indicates that class A and B Hsp40 chaperones function in tandem with Hsp70 and an Hsp70 nucleotide-exchange factor, Hsp110, to solubilize small aggregates both in vitro and in vivo (Nillegoda *et al.*, 2015, 2017; Kirstein *et al.*, 2017). In addition, Hsp40s are one of the largest families of Hsps, and mammalian cells express >50 family members. This network of Hsp70 cofactors has expanded during evolution to accommodate the concomitant increase in the number of substrates in more complex organisms, and thus their roles are critical for the maintenance of protein homeostasis, or "proteostasis" (Rebeaud *et al.*, 2021). To date, however, only one Hsp40 in the ER membrane, with an ER lumenal-facing J domain, has been shown to facilitate ApoB degradation (Oyadomari *et al.*, 2006; Rutkowski *et al.*, 2007). In contrast, the role of cytosolic Hsp40s in ApoB ERAD has never been explored.

Based on the importance of preventing ApoB aggregation before proteasome delivery, we set out to examine if cytosolic class A and B Hsp40s facilitate ApoB solubility and then target ApoB for ERAD. By using a yeast model we previously established (Hrizo *et al.*, 2007; Grubb *et al.*, 2012; Doonan *et al.*, 2019), as well as a rodent cell line that endogenously synthesizes and secretes ApoB-containing lipoproteins, we observed—as anticipated—that class A (DNAJA1) and class B Hsp40 (DNAJB1) associate with ApoB. We then found that the class A Hsp40 facilitates ApoB degradation, but surprisingly the class B Hsp40 instead stabilizes the apolipoprotein. Yet, in line with these unexpected results, the ablation of the class A Hsp40 led to the accumulation of ubiquitinated ApoB, whereas class B knockdown decreased the levels of ubiquitinated ApoB. These data suggest that the chaperones act at different steps during ApoB maturation and more generally indicate for the first time that substrate-associated Hsp40s can play opposing roles during ERAD.

RESULTS

The ER-associated Hsp40, Ydj1, and the Ssa1 Hsp70 chaperone facilitate ApoB ERAD in yeast

Prior work established that cytoplasmic Hsp70 is required for ApoB degradation (Fisher *et al.*, 1997; Gusarova *et al.*, 2001). This discovery was made possible in part through the development of a system in which the contributions of reagents isolated from yeast cells and cell culture systems could be investigated in vitro (Gusarova *et al.*, 2001). To test if Hsp40s also oversee ApoB stability—and to confirm that yeast Hsp70 is required for ApoB ERAD when expressed in this model organism—we utilized a *Saccharomyces cerevisiae* β-estradiol inducible expression system (Doonan *et al.*, 2019). In brief, yeast strains were transformed with a linearized plasmid encoding a chimeric transcription factor, pACT1-GEV, and cells were selected in which the construct was stably integrated (McIsaac *et al.*, 2011). This chimeric transcription factor is composed of a GAL4 DNA-binding domain, an estrogen-binding domain, and the VP16 transcription factor. The GEV chimeric transcription factor is constitutively expressed under the control of an ACT1 promoter but remains inactive in the cytosol and bound to Hsp90. Once β-estradiol is added, the hormone targets the estrogen receptor domain in GEV, thus releasing the Hsp90 repressor. The liberated GEV enters the nucleus, binds the upstream sequence of GAL promoters, and rapidly activates transcription of GAL-regulated genes.

To establish the anticipated role of Hsp70 in facilitating the ERAD of ApoB in yeast, we conducted cycloheximide chase assays in the *ssa1-45* strain, which lacks the homologous *SSA2*, *SSA3*, and *SSA4* genes and is viable at permissive temperatures due to the presence of a thermosensitive *SSA1* allele (Becker *et al.*, 1996). An isogenic strain containing a wild-type copy of *SSA1* served as a control. The

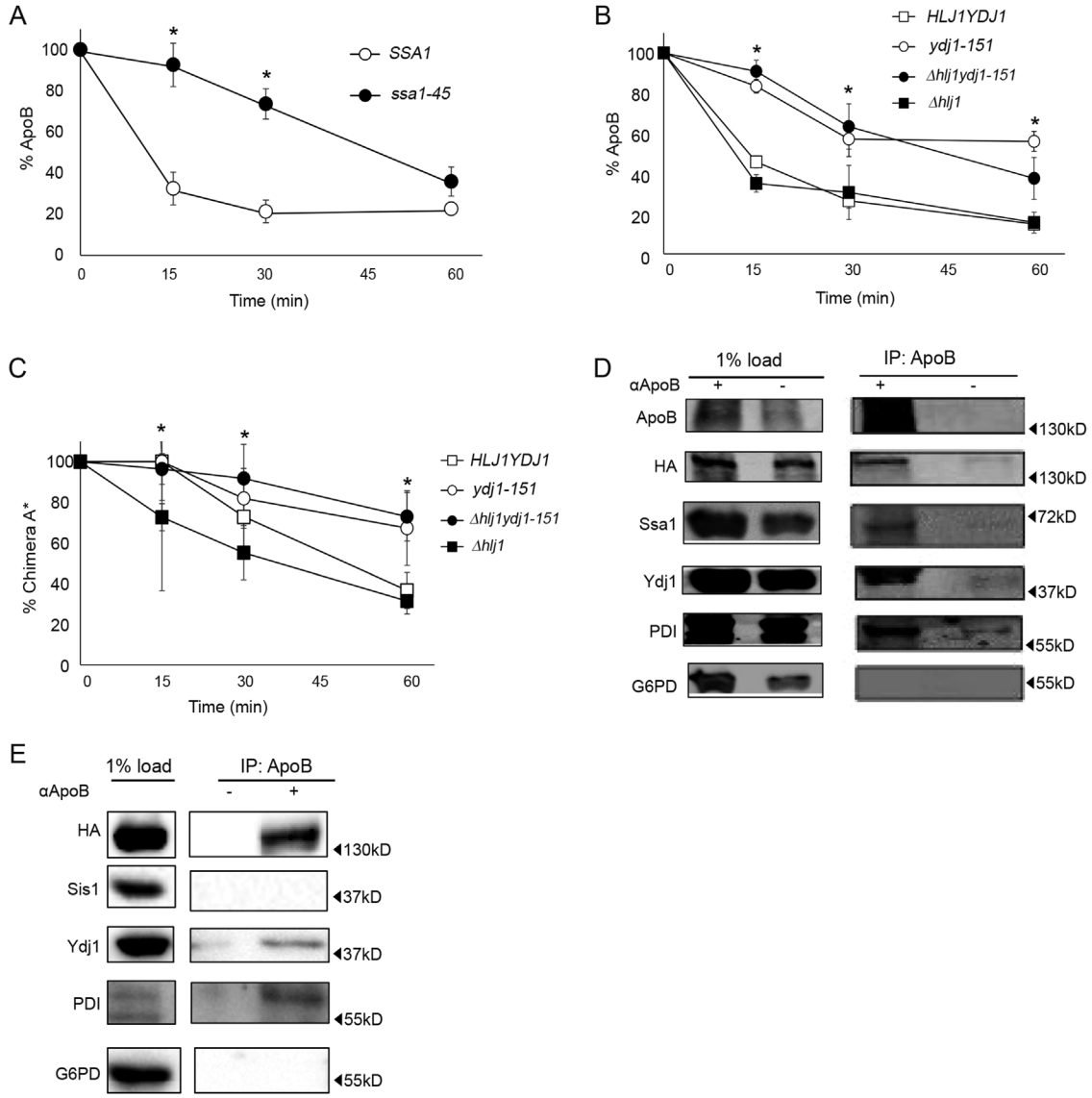

FIGURE 1: Ydj1 associates with and facilitates the degradation of ApoB29. (A) Cycloheximide chase assays were conducted as described in the *Materials and Methods*. The turnover of ApoB was examined in *SSA1* (open circle) and *ssa1-45* (closed circle) strains expressing ApoB29 after cells had been shifted to 37°C for 30 min and β-estradiol was present for 1 h. Equivalent ODs of cells were collected at the indicated time points and processed for quantitative Western blotting. Data from each time point were normalized to the G6PDH loading control. The amount of ApoB29 remaining over time was plotted relative to the amount of protein at time 0. (B) Cycloheximide chase assays were conducted in the *HLJ1YDJ1* (open square), *Δhlj1* (closed square), *ydj1-151* (open circle), and *Δhlj1ydj1-151* (closed circle) strains expressing ApoB29 as described above. (C) Cycloheximide chase assays were again conducted in each strain but in this case the yeast expressed a model ERAD substrate, Chimera A*, whose turnover is known to similarly require Ydj1 function. (D) Coimmunoprecipitation assays were performed as described in the *Materials and Methods* using an antibody against ApoB in wild-type cells expressing HA-tagged ApoB29, and precipitated proteins were subject to immunoblot analysis with the indicated antibodies. Note the presence of ApoB29 as well as the Ssa1, Ydj1, and PDI molecular chaperones in the "IP: ApoB" lane from the antibody-treated (+) sample. (E) Coimmunoprecipitation assays were performed as described in the *Materials and Methods* and in Figure 1D. In panels A–C, data were calculated from $N = 5$ independent experiments, ±SE, $*p < 0.05$. Statistical significance was calculated by Student's unpaired *t* test.

version of ApoB used for this analysis contains the N-terminal 29% of the protein, which is the smallest fragment capable of transiting through the secretory pathway and is still metabolically regulated in higher eukaryotes (Collins *et al.*, 1988; Linton *et al.*, 1993; McLeod *et al.*, 1994). After ACT1-GEV versions of *SSA1* and *ssa1-45* yeast strains were generated, a cycloheximide chase assay was performed after cells had been shifted for 30 min to 37°C. Consistent with data from mammalian cells and in vitro (Fisher *et al.*, 1997; Gusarova *et al.*, 2001), the initial rate of ApoB29 degradation was significantly slowed in *ssa1-45* yeast (Figure 1A).

We next explored the contributions of two cytosolic ER-associated Hsp40s with established roles in ERAD. Yeast express >20 Hsp40 isoforms (Kampinga and Craig, 2010; Kampinga *et al.*, 2019), but of the dozen or so Hsp40s present in the cytosol, only Hlj1 and Ydj1 are associated with the ER membrane. Whereas Hlj1, a class B Hsp40, embeds into the ER membrane due to a C-terminal tail anchor, Ydj1,

a class A Hsp40, is tethered to the lipid bilayer by a farnesyl moiety (Cyr *et al.*, 1992; Becker *et al.*, 1996; Hoe *et al.*, 1998; Costanzo *et al.*, 2001; Beilharz *et al.*, 2003; Walsh *et al.*, 2004). Therefore to specifically examine the contributions of Ydj1 and Hlj1 on ApoB stability, we used strains in which the gene encoding Hlj1 was deleted (*Δhlj1*) and/or that contained a temperature-sensitive *YDJ1* allele (*ydj1-151*) since—in some backgrounds—the Ydj1 protein is essential (Caplan and Douglas, 1991; Cyr and Douglas, 1994). Next, GEV-expressing yeast were isolated and the temperature sensitivity of cells containing the *ydj1-151* allele was confirmed (unpublished data). The ApoB29 plasmid was then introduced into the yeast and after β-estradiol was added for 1 h, the strains were shifted to 37°C. As shown in Figure 1B, ApoB29 was only stabilized in strains containing the loss-of-function mutation in Ydj1 (i.e., the *ydi1-151* and *Δhlj1 ydj1-151* strains). We also ensured that a known ERAD substrate was stabilized in the GEV-integrated strains. To this end, each strain was transformed with a plasmid engineered to express Chimera A*, an ERAD substrate whose degradation requires Ydj1 (Preston *et al.*, 2018). Consistent with previous findings, Chimera A* degradation was slowed only in the *ydj1-151* and *Δhlj1 ydj1-151* strains (Figure 1C).

Besides stimulating and enhancing the ATPase activity of Hsp70s, Hsp40s aid in substrate recognition (Fan *et al.*, 2003; Craig and Marszalek, 2017). To explore if Ydj1 identifies ApoB29 for ERAD, we conducted coimmunoprecipitation experiments. After cell lysis and antibody-associated precipitation, the presence of ApoB29 and distinct chaperones and other proteins in the precipitate was examined by Western blotting. ApoB29 coimmunoprecipitated with Ydj1 and to a lesser degree Ssa1, and as a positive control we found that PDI was ApoB associated (Figure 1, D and E), as previously reported (Grubb *et al.*, 2012). In contrast, G6PDH, a cytosolic enzyme, was absent after precipitation. As a negative control for this experiment, we also examined if Sis1, which thus far has not been associated with the ERAD pathway, also precipitates with ApoB. As anticipated, Sis1 was absent from the ApoB-containing complex, in contrast to Ydj1 as well as PDI (Figure 1E). These data suggest that Ydj1 interacts with and regulates the ERAD of ApoB in yeast.

The DNAJA1 molecular chaperone associates with and facilitates the degradation of ApoB100 in mammalian cells

Among the model systems used to study ApoB biology, McArdle cells, a rat hepatoma cell line, are ideal because they endogenously express and secrete lipidated ApoB100 that resembles VLDL (Meex *et al.*, 2011). The cells also faithfully recapitulate ApoB degradation under lipid-poor conditions. Moreover, specific candidate genes can be readily knocked down or overexpressed and their effects on ApoB100 stability and transport examined in pulse-chase experiments (Bostrom *et al.*, 1986; Borchardt and Davis, 1987; Boren *et al.*, 1992, 1994).

We began by examining the effects of knocking down DNAJA1 (also known as Hdj2) since this is one of the closest mammalian homologues of Ydj1 (~46% sequence identity; see Supplemental Figure S1). Like Ydj1, DNAJA1 is also a class A Hsp40 (Stark *et al.*, 2014; Craig and Marszalek, 2017). To optimize knockdown conditions, we tested five ORF-targeted siRNA oligonucleotides at several concentrations and at two time points post-transfection. In addition, since DNAJA1 modulates the biogenesis of select substrates (Okiyoneda *et al.*, 2011; Abisambra *et al.*, 2012; Rauch and Gestwicki, 2014; Dekker *et al.*, 2015; De Mattos *et al.*, 2020), we confirmed that knockdown failed to elicit a general stress response by measuring Hsp70 levels (see *Materials and Methods* and Supplemental Figure S2A). Under the final optimized conditions, DNAJA1 was reduced to ~20% of the levels present in the scrambled siRNA control (Figure 2A). This extent of knockdown is in line with other studies in which the effect of DNAJA1 was measured after silencing (see Meshalkina *et al.*, 2016; Parrales *et al.*, 2016). We then conducted pulse-chase experiments in the presence of the scrambled siRNA or after knocking down DNAJA1 (Figure 2, B and C). In the control, ApoB100 was present in cell lysates after 15 min, and the protein was secreted after 60 min, consistent with published data (Bostrom *et al.*, 1986; Boren *et al.*, 1992, 1994; White *et al.*, 1992). This delay reflects the fact that ApoB100 requires ~30 min to be synthesized, folded, packaged into COPII vesicles for transport to the Golgi, and secreted (Benoist and Grand-Perret, 1997).

Next, we measured ApoB100 levels and stability over time. When DNAJA1 was silenced, both the intracellular and especially the secreted ApoB100 levels rose significantly compared to the scrambled siRNA control at both the 60- and 90-min time points (Figure 2, B and C; see closed arrowheads and graphs). The magnitude of this effect was mirrored by the increase in ApoB100 achieved when the proteasome is inhibited (Liang *et al.*, 2000; Cardozo *et al.*, 2002; Fisher *et al.*, 2008) (also see gray bars, Figure 2D). This result suggests that DNAJA1 helps deliver ApoB100 to the ERAD pathway. Consistent with this view, combined knockdown of DNAJA1 and treatment with MG132 failed to further increase ApoB100 levels (Figure 2D).

To ensure that DNAJA1 depletion did not affect the biogenesis of all proteins that traverse the secretory pathway, we also measured albumin secretion from McArdle cells treated under control or DNAJA1 knockdown conditions. First, we confirmed that the DNAJA1 siRNA again led to profound depletion of the chaperone, yet neither actin nor Hsp70 levels were altered (Figure 2A and Supplemental Figure S2A). Next, albumin was immunoprecipitated from a lysate fraction that contained equal radioactive counts 15 and 60 min into chase. As shown in Supplemental Figure S2B, the levels of secreted albumin were identical, regardless of whether DNAJA1 was abundant.

Because Ydj1 coimmunoprecipitates with ApoB29 in yeast (Figure 1, D and E), we asked if DNAJA1 also binds ApoB100 in McArdle cells. To this end, cells were treated with the membrane-permeable chemical crosslinker, dithiobis(succinimidyl propionate) (DSP) (Mattson *et al.*, 1993), and after solubilization under denaturing conditions, ApoB100 was immunoprecipitated with an antibody directed against the protein along with Protein G–Sepharose. Protein partners were identified by Western blotting. As displayed in Figure 2E (IP +ab), DNAJA1 was cross-linked to ApoB100. In contrast, an interaction was absent between the apolipoprotein and actin.

The solubility of ApoB is unaffected when DNAJA1 is depleted

Based on the action of other Hsp40s (Kampinga *et al.*, 2019) and the fact that DNAJA1 binds ApoB100, we asked if DNAJA1 might act as a "holdase" to maintain ApoB100 solubility as it retrotranslocates from the ER en route to the proteasome. A cellular holdase might be critical given the highly hydrophobic nature of the protein (Segrest *et al.*, 1992). Therefore a series of detergent solubility assays using a nonionic detergent, dodecyl maltoside (DDM), which solubilizes membrane integrated proteins but not aggregated proteins (Calcutta *et al.*, 2012), was conducted. Lysates prepared from cells treated with the control or an siRNA directed against DNAJA1 were incubated with a range of DDM concentrations on ice, the samples were centrifuged at 100,000 × *g*, the soluble (supernatant) and insoluble (pellet) fractions were processed, and the presence of ApoB100 and ribophorin, an integral ER membrane protein control (Crimaudo *et al.*, 1987), was examined by Western blot analysis.

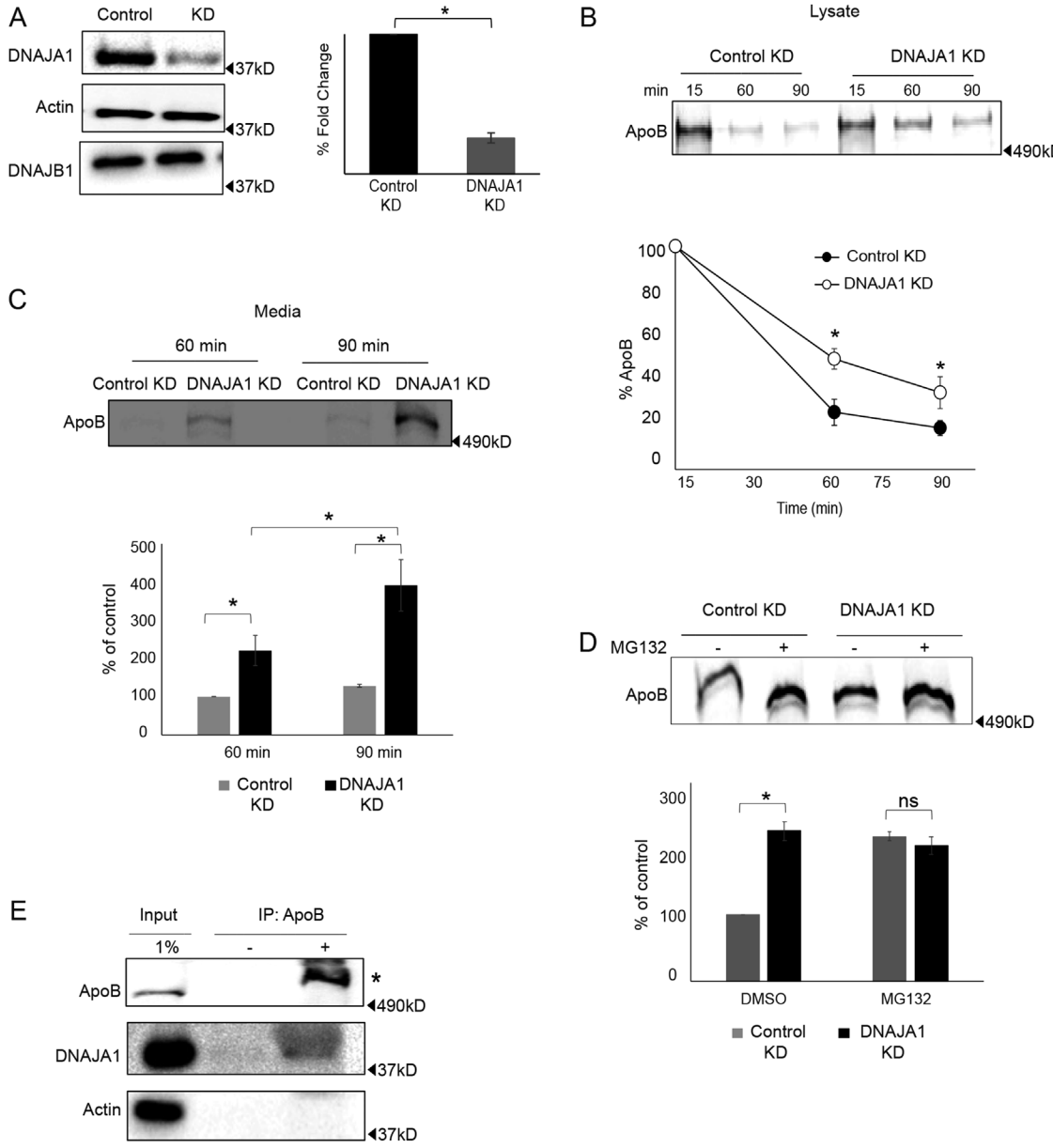

FIGURE 2: The DNAJA1 molecular chaperone facilitates ApoB100 degradation. (A) McArdle cells were transfected with the most efficacious DNAJA1 siRNA (KD) or a scrambled siRNA (control) for 48 hr. A representative Western blot shows DNAJA1, DNAJB1, and actin levels after knockdown. (B) A pulse-chase experiment was conducted as described in the *Materials and Methods* after cells were starved for 1 h and then incubated with radioactive Met/Cys for 15 min (pulse). ApoB100 was immunoprecipitated using an anti-ApoB antibody and analyzed via SDS–PAGE and phosphorimaging analysis. A representative radiograph and graph of the intracellular ApoB100 levels over time are shown. (C) A representative radiograph and graph show the levels of secreted ApoB100 over time. (D) DNAJA1 was either knocked down and/or cells were treated with MG-132 for 1 h before a pulse-chase analysis was conducted. A representative radiograph shows ApoB100 levels under each condition. (E) Chemical cross-linking was performed as described in the *Materials and Methods* after cells were treated with 2 mM DSP for 30 min. Input (1%) and immunoprecipitated fractions were processed for SDS–PAGE and Western blotting. Actin was used as a negative control. The slower migration of the cross-linked immunoprecipitated ApoB100 indicates incomplete reduction of the cross-linked complex in the immunoprecipitated fraction (denoted with an asterisk). In panels A-D, data represent the means of $N = 5$ independent experiments, ±SE; *$p < 0.05$, ns indicates $p > 0.05$. Statistical significance was calculated by Student's unpaired *t* test.

Contrary to our hypothesis, depletion of DNAJA1 had no effect on ApoB100 solubility (Supplemental Figure S3A). Similar results were obtained when a range of other detergents were examined in control or DNAJA1-depleted cells (i.e., NP-40, sodium deoxycholate, Triton X-100) and under a variety of conditions (unpublished data). However, when the solubility of the cystic fibrosis transmembrane conductance regulator, CFTR, an established aggregation-prone protein (Strickland *et al.*, 1997; Estabrooks and Brodsky, 2020), was measured, the protein resided primarily in the insoluble pellet (P) in detergent-treated lysates (Supplemental Figure S3B). These data suggest that DNAJA1 facilitates ERAD independent of its potential solubilizing effects.

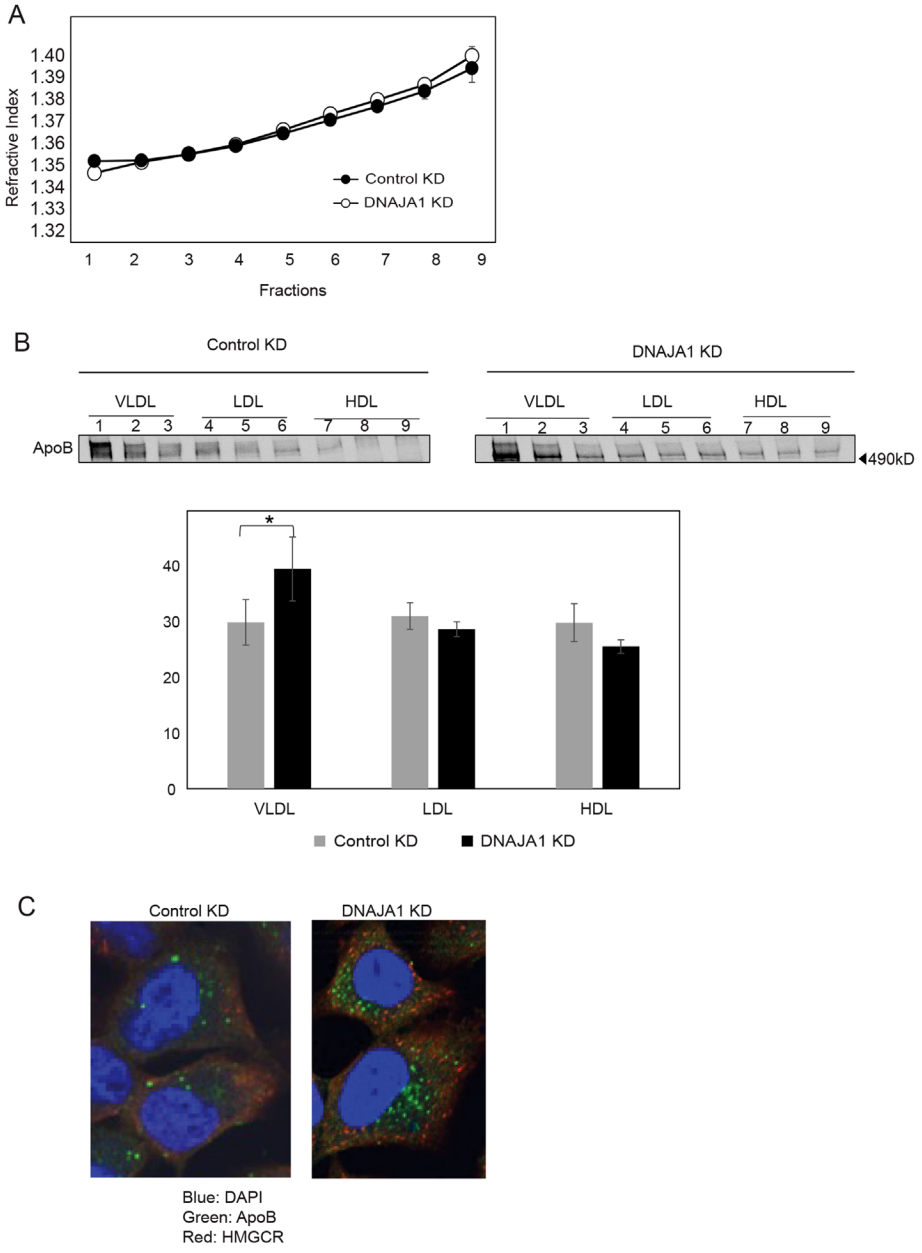

FIGURE 3: Depletion of DNAJA1 increases ApoB100 lipidation and ApoB100 puncta formation. McArdle cells were treated with an siRNA against DNAJA1 (DNAJA1 KD) or a scrambled control (Control KD), pulse labeled with radioactive Met/Cys for 15 min, and after the media were changed, an excess of unlabeled amino acids was provided. The media were then collected after 90 min into the chase and subjected to sucrose gradient ultracentrifugation before the indicated fractions were collected. (A) Refractive indices were measured for each fraction. (B) ApoB100 was precipitated from each fraction and processed by SDS–PAGE and phosphorimage analysis. The graph represents the relative amount of ApoB100 residing in VLDL (0.95–1.006 g/ml), LDL (1.006–1.063 g/ml), and HDL (1.063–1.210 g/ml) in the precipitated fractions. Data represent the means of $N = 3$ independent experiments, ±SE. (C) Confocal IF images from McArdle cells probed with antibodies against ApoB (green) and the smooth ER resident protein, HMG-CoA reductase (red). DAPI staining (nucleus) is also shown. Statistical significance was calculated by Student's unpaired *t* test.

DNAJA1 deficiency increases ApoB100 lipidation

The secreted ApoB100 pool in serum normally contains fully lipidated lipoprotein particles (Boren *et al.*, 1994), and in cell culture a range of particles can be detected, including VLDL, LDL, and HDL (Meex *et al.*, 2011). Because DNAJA1 silencing enhanced ApoB100 secretion, we asked if ApoB100 was lipid-depleted under these conditions since the secreted pool might otherwise have been targeted for ERAD, or if the rescued ApoB100 remained accessible to MTP and the post-ER lipidation machinery (Gusarova *et al.*, 2003). To measure the extent of secreted ApoB100 lipidation, we followed an established protocol (Boren *et al.*, 1992, 1994; Sparks *et al.*, 1992; Wang *et al.*, 1993). First, DNAJA1 was knocked down or cells were treated with a scrambled siRNA control, as above. This step was followed by a pulse-chase analysis, and media samples were collected 90 min into the chase. Normalized radioactive counts from the media of the control and experimental cells were then diluted and overlaid on a 12.5–50% sucrose gradient, and after centrifugation to equilibrium (~65 h), 12 fractions were collected and ApoB100 was immunoprecipitated from each fraction. We also measured the refractive index of each fraction along with a series of controls that together confirmed gradient integrity and identified the predicted positions at which VLDL- and LDL-like particles migrate (Figure 3A). Consistent with the second model above, DNAJA1 depletion resulted in the production of a slightly greater percentage of the most buoyant, lipid-rich particles that were VLDL-like (≤ 1.006 g/ml) (Smith *et al.*, 1978; Tiwari and Siddiqi, 2012) (Figure 3B). Based on this result, we propose that DNAJA1 depletion slows ERAD, increases the efficiency of cotranslational translocation, and thus augments MTP association and lipid loading (i.e., VLDL assembly; also see *Discussion*). Of note, the relatively modest effect observed in the VLDL pool most likely reflects the fact that a significant amount of ApoB100 is still targeted for degradation even after DNAJA1 is depleted (Figure 2D).

Under steady-state conditions and in the absence of excess exogenous lipids, ApoB most commonly forms puncta that reside in both the ER and in the post-ER compartments (Fisher *et al.*, 1997; Mitchell *et al.*, 1998; Butkinaree *et al.*, 2014). Consistent with enhanced ApoB100 flux through the secretory pathway (Figure 2), DNAJA1 deficiency led to an apparent increase in the number and sizes of ApoB100 puncta in McArdle cells. As anticipated, ApoB100 residence was also distinct from HMG-CoA reductase, a component of the smooth ER (Figure 3C).

DNAJB1, a class B Hsp40, also associates with but instead stabilizes ApoB100

Hsp70s can have multiple Hsp40 partners, and heterologous pairs of Hsp40 isoforms are common (Liu *et al.*, 2020). Moreover, class A and class B JDPs function with Hsp70 and Hsp110 family members to act as components of protein disaggregases (Nillegoda *et al.*, 2017;

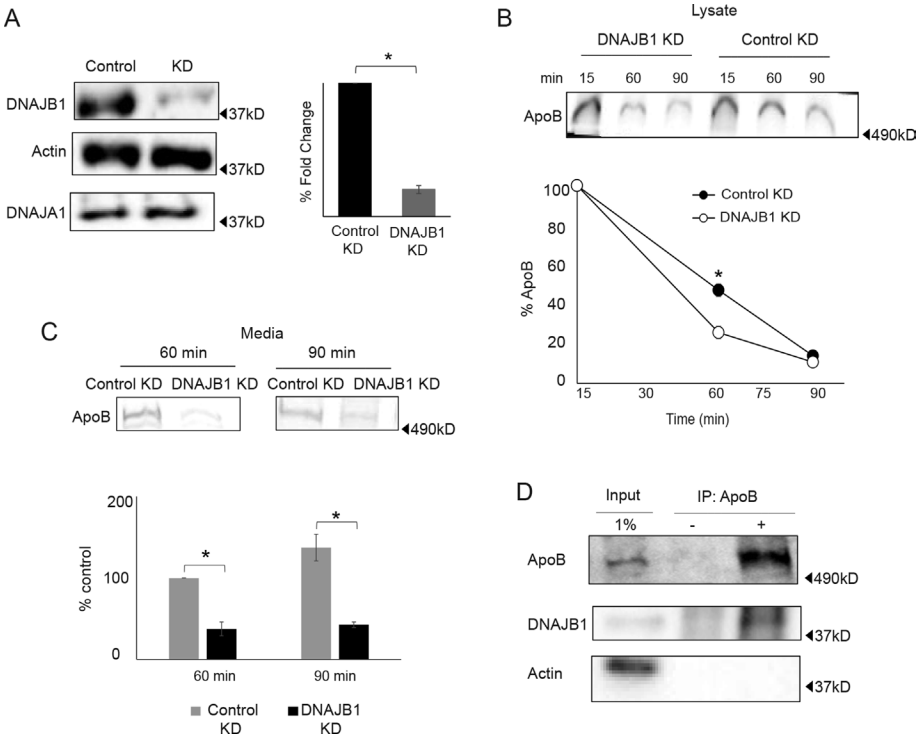

FIGURE 4: The DNAJB1 molecular chaperone augments ApoB100 biogenesis. (A) McArdle cells were transfected with the most efficacious DNAJB1 siRNA (KD) or a scrambled siRNA (Control) for 48 hr. A representative Western blot shows DNAJB1, DNAJA1, and actin levels after knockdown. (B) A pulse-chase experiment was conducted as described in the *Materials and Methods* and in Figure 2. A representative radiograph and graph of intracellular ApoB100 levels over time are shown. (C) A representative radiograph and graph show the levels of secreted ApoB100 over time. (D) Chemical cross-linking was performed as described in the *Materials and Methods* and in Figure 2E. Actin was used as a negative control. Data represent the means of $N = 5$ independent experiments, ±SE; $*p < 0.05$. Statistical significance was calculated by Student's unpaired *t* test. The mean of the data ± SD was also significant for time point 60 min in B.

Nillegoda *et al.*, 2018; Wentink *et al.*, 2020). In yeast, an alternate disaggregase is Hsp104 (Parsell *et al.*, 1994). Hsp104 functions in tandem with Hsp70-Hsp40 (Glover and Lindquist, 1998), and prior work from our lab demonstrated that Hsp104 associates with and facilitates the degradation of ApoB29 in the yeast model (Doonan *et al.*, 2019). Although DNAJA1 depletion did not alter ApoB100 solubility (Supplemental Figure S3) while supporting ERAD, we still anticipated that a class B Hsp40 that associates with DNAJA1 would similarly facilitate ERAD. To this end, we investigated the contribution of DNAJB1 (also known as Hdj1) on ApoB100 biogenesis. Notably, DNAJA1 and DNAJB1 interact as components of cellular protein disaggregases (Nillegoda *et al.*, 2015, 2017, 2018; Kirstein *et al.*, 2017; Wentink *et al.*, 2020).

As above, we first optimized DNAJB1 knockdown conditions in McArdle cells (see *Materials and Methods* and unpublished data). Ultimately, a knockdown efficiency of ~80% was achieved (Figure 4A), and as observed when DNAJA1 was silenced (Figure 2A), the depletion of DNAJB1 had no effect on Hsp70 steady-state levels (unpublished data). The amounts of DNAJA1 and actin were also unchanged (Figure 4). Next, the stability of ApoB100 was examined in pulse-chase assays using cells treated with the scrambled siRNA control or the siRNA directed specifically against DNAJB1. In this case—and unexpectedly in contrast to the effect of DNAJA1 depletion—DNAJB1 knockdown failed to slow ApoB100 turnover. Instead, there was ~2-fold less ApoB100 in cells at the 60-min time point (Figure 4B; please note that the error bars are obscured by the symbol). There was also a pronounced ~4-fold decrease in the amount of secreted ApoB100 compared with the control at both the 60- and 90-min time points (Figure 4C), suggesting that higher levels of secretion were maintained after the initial buildup of cellular ApoB100. This result also indicates that the lower level of ApoB100 in cells (Figure 4B) cannot be explained by increased secretion when DNAJB1 was silenced. A direct effect of DNAJB1 on ApoB100 biogenesis was further supported by the fact that DNAJB1 could be cross-linked to ApoB (Figure 4D), yet like DNAJA1, the knockdown of DNAJB1 also failed to alter ApoB100 solubility (Supplemental Figure S4). Thus, in contrast to the role that DNAJA1 plays in enhancing degradation, DNAJB1 appears to instead facilitate ApoB100 folding/maturation in the ER (but see below).

Neither a class C Hsp40 nor another class B Hsp40 associate with ApoB100

To control for these knockdown experiments, the potential effect of a JDP that resides in another cellular compartment—yet is linked to proteostasis—was measured. We selected a class C Hsp40, DNAJC19, which resides in the inner mitochondrial membrane. DNAJC19 functions during protein translocation into the mitochondria (Heinemeyer *et al.*, 2019), so defects might lead to cytoplasmic stress responses. In fact, mutations in the gene encoding this chaperone result in cardiomyopathy with ataxia (Janz *et al.*, 2020). Therefore we followed the same experimental methods outlined above and again optimized DNAJC19 knockdown conditions. However, as shown in Supplemental Figure S5A, DNAJC19 knockdown was nearly complete but had no effect on the intracellular or secreted levels of ApoB100 (Supplemental Figure S5, B and C). Chemical cross-linking with DSP also indicated that DNAJC19 fails to associate with ApoB100 (Supplemental Figure S5D). As an additional negative control, we examined whether another class B cytoplasmic Hsp40, DNAJB6, cross-links to ApoB100. Although this chaperone is known to be involved in modulating the formation of protein aggregates and amyloids (Thiruvalluvan *et al.*, 2020), DNAJB6 also failed to associate with ApoB100, in contrast to DNAJA1 and Hsp70 (Supplemental Figure S6).

DNAJA1 and DNAJB1 differentially alter ApoB100 ubiquitination

In some cases, Hsp40s select ERAD substrates prior to substrate ubiquitination, so Hsp40 depletion can correlate with reduced ubiquitination (Nakatsukasa *et al.*, 2008; Preston and Brodsky, 2017). Because DNAJA1 depletion slowed ApoB100 degradation (Figure 2), we initially suspected that the chaperone would similarly act prior to ApoB100 ubiquitination and, therefore, that DNAJA1 silencing would decrease ubiquitin conjugation. To test this hypothesis, ApoB100 ubiquitination was examined in lysates from cells transfected with a ubiquitin overexpression plasmid and incubated

in the presence or absence of MG132. After lysis, ApoB100 was immunoprecipitated, and ubiquitinated ApoB100 levels were analyzed by Western blotting. In contrast to our hypothesis, ubiquitinated ApoB100 accumulated when DNAJA1 was knocked down (see DMSO samples, left, Figure 5A). This result suggests that DNAJA1 acts after substrate ubiquitination in the ERAD pathway, perhaps by facilitating ApoB100 delivery to the proteasome (also see *Discussion*). As a control for this experiment, there was no effect on ApoB100 ubiquitination when DNAJC19 was depleted (Figure 5, A and D). Moreover, MG132 increased the amount of ubiquitinated ApoB100 in both knockdown and control conditions (Figure 5, A and B), consistent with the targeting of ubiquitin-modified ApoB100 to the proteasome, as well as with the data in Figure 2D.

In contrast to the effect of DNAJA1 ablation, DNAJB1 knockdown decreased ApoB100 ubiquitination in the absence of MG132 (DMSO, left, Figure 5, A and C). Nevertheless, the addition of MG132 magnified the level of ApoB100 ubiquitination to an equal degree, regardless of whether DNAJB1 was silenced (Figure 5C). This result suggests that DNAJA1 and DNAJB1 act at different stages during ApoB100 biogenesis, in accordance with their distinct effects on substrate stability. In contrast to these results, prior work indicated that DNAJB1 knockdown had no effect on the ubiquitination and degradation of mutant p53 (Parrales *et al.*, 2016), but in another study there was an increase in mitogen inducible gene 6 (MIG6) ubiquitination when DNAJB1 was silenced (Park *et al.*, 2015). Overall, these and other data highlight the varied roles that Hsp40s can play during ERAD and, more generally, on the maintenance of cellular proteostasis (see below).

DISCUSSION

ApoB100 is an atypical ERAD substrate. This large (~550 kDa) apolipoprotein contains pause-transfer sequences, is ubiquitinated cotranslationally, and is regulated by presecretory degradation via the ERAD pathway (Boren *et al.*, 1992, 1994; Yeung *et al.*, 1996; Benoist and Grand-Perret, 1997; Fisher *et al.*, 1997; Sakata *et al.*, 1999; Brodsky and Fisher, 2008). Even though cytosolic Hsp70 has been known for many years to regulate ApoB100 turnover (Fisher *et al.*, 1997; Gusarova *et al.*, 2001), cytosolic Hsp40s that modify the stability of ApoB have not been reported.

In this study, we identified and characterized the roles of two ER-associated Hsp40s that regulate ApoB100 biogenesis in McArdle cells. We began by conducting a candidate-based screen in a yeast ApoB29 expression system. Yeast express approximately a dozen Hsp40 homologues, but by focusing on those linked to ERAD we discovered that Ydj1, a Class A Hsp40, associates with and facilitates ApoB29 degradation (Figure 1). While it is noteworthy that the absence of another JDP (i.e., Hlj1) had no effect on ApoB stability, and that no interaction with yet another homolog was apparent (i.e., Sis1), we acknowledge that additional Hsp40s might act with or in opposition to Ydj1. Indeed, in one study it was shown that only 4/13 of the yeast Hsp40s exhibited "specialty" functions (Sahi and Craig, 2007). Next, since prior efforts established that data from the yeast model can be translated into mammalian cell systems (Hrizo *et al.*, 2007; Grubb *et al.*, 2012), we investigated the effects of DNAJA1, a mammalian Ydj1 homolog, on ApoB100 biogenesis in a rodent hepatic cell line that synthesizes and secretes ApoB100. Consistent with data in yeast, DNAJA1 similarly associated with and facilitated the ERAD of ApoB100. Because Hsp40s regulate ERAD either before or after ubiquitination (Brodsky, 2007; Preston and Brodsky, 2017), we also asked if ApoB100 was ubiquitinated to a greater or lesser extent on DNAJA1 depletion. Ubiquitinated ApoB100 accumulated when DNAJA1 was silenced (Figure 5), suggesting that the

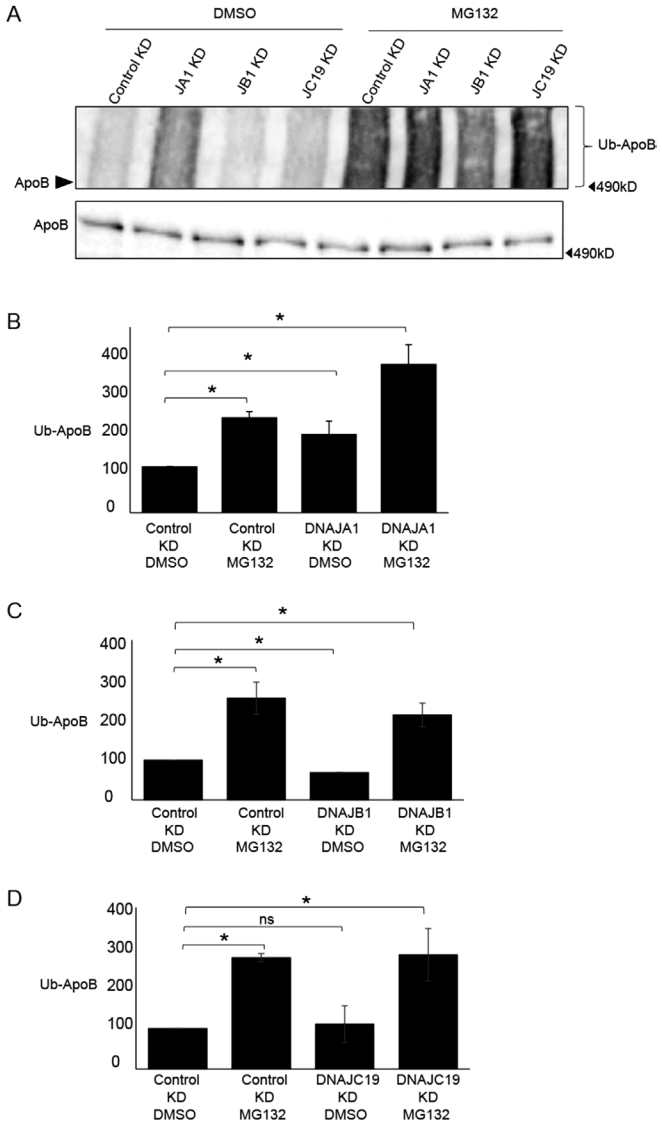

FIGURE 5: The depletion of DNAJA1 and DNAJB1 leads to opposite effects on the levels of ubiquitinated ApoB100. (A) ApoB100 ubiquitination was assayed in McArdle cells that also transiently expressed HA-tagged ubiquitin and were treated in the presence of a control siRNA or an siRNA directed to DNAJA1, DNAJB1, or DNAJC19 as described in the *Materials and Methods*. Cells were also pretreated with DMSO or MG132 for 1 h before they were lysed and ApoB100 was immunoprecipitated. The levels of ubiquitinated ApoB100 (Ub-ApoB) were detected via SDS–PAGE and Western blotting against ApoB100 and HA (to detect the ubiquitinated protein). A representative Western blot shows the levels of ubiquitinated Apo100. The arrowhead denotes the migration of unmodified ApoB100 at ~550 kDa. (B–D) Graphs show the levels of ubiquitinated ApoB100 normalized to the corresponding levels of ubiquitinated ApoB100 in the presence of DMSO and in cells that had been treated with the scrambled (control KD) siRNA. Data represent the means of $N = 5$ independent experiments, ±SE; $^*p < 0.05$, ns indicates $p > 0.05$. Statistical significance was calculated by Student's unpaired *t* test.

chaperone acts after the gp78 ubiquitin ligase (Liang *et al.*, 2003a) has modified ApoB100. Because chaperones, including Hsp40s, play critical roles in maintaining protein solubility, we also investigated if DNAJA1 depletion alters ApoB solubility, but no change in detergent solubility was noted after chaperone levels fell. These

results suggest that DNAJA1 is dispensable for ApoB100 disaggregation and plays another role during ApoB turnover, perhaps facilitating the transfer of ApoB100 to the proteasome. Indeed, prior studies have suggested that the proteasome can serve as a platform for chaperones that participate in the transfer of ubiquitinated proteins (Verma *et al.*, 2000). It thus remains likely that there are other compensatory disaggregases—or even other Hsp40s—that facilitate ApoB100 solubility (also see above). This hypothesis will be examined in future studies.

The decision to either degrade or secrete ApoB100 is made at the ER/cytosol interface and is tightly regulated. This mechanism represents a tug-of-war between ER lumenal factors that favor lipoprotein assembly (e.g., Hsp110 and the MTP complex) and cytosolic components that target ApoB100 for degradation (e.g., Hsp70, Hsp90, Hsp104, p58^{IPK}) (Boren *et al.*, 1992, 1994; Benoist and Grand-Perret, 1997; Fisher *et al.*, 1997; Gusarova *et al.*, 2001; Hrizo *et al.*, 2007; Grubb *et al.*, 2012; Sirwi and Hussain, 2018; Doonan *et al.*, 2019;). Because ApoB100 achieves a bi-topic orientation with respect to the ER membrane while undergoing cotranslational translocation, the apolipoprotein remains in close proximity to DNAJA1, which is anchored to the ER membrane (Cyr *et al.*, 1992; Becker *et al.*, 1996; Hoe *et al.*, 1998; Terada and Mori, 2000; Costanzo *et al.*, 2001; Beilharz *et al.*, 2003; Walsh *et al.*, 2004; Xu *et al.*, 2019). p97/VCP has also been shown to coimmunoprecipitate with ApoB100 and facilitate ApoB100 degradation (Fisher *et al.*, 2008; Rutledge *et al.*, 2009), suggesting that DNAJA1 assists p97/VCP during retrotranslocation after the apolipoprotein is ubiquitinated. Therefore DNAJA1 depletion might increase the extent of cotranslational translocation, folding, and lipidation by the MTP complex, which favors transit into the ER lumen. This would explain the fact that DNAJA1 knockdown increased ApoB100 buoyancy/lipidation.

DNAJA1 is member of an interclass JDP complex (Nillegoda *et al.*, 2015, 2017, 2018; Kirstein *et al.*, 2017; Wentink *et al.*, 2020), so we anticipated that DNAJB1, a class B Hsp40, would also play a role in ApoB100 degradation. Contrary to our hypothesis, DNAJB1 knockdown accelerated ApoB100 turnover, suggesting that the chaperone is an ApoB100 stabilizer. As observed with DNAJA1, DNAJB1 also cross-linked to ApoB100, but in contrast to DNAJA1, DNAJB1 depletion blunted ApoB100 ubiquitination. While initially unexpected, this result is consistent with the functional diversity noted among Hsp40s and even with their different effects on a range of substrates. For example, DNAJA1 and DNAJB1 aid in CFTR folding, but DNAJB12 and DNAJC5 facilitate its degradation (Meacham *et al.*, 1999; Farinha *et al.*, 2002; Zhang *et al.*, 2002; Schmidt *et al.*, 2009;). In turn, DNAJA1 knockdown decreases the maturation efficiency of the hERG channel (Walker *et al.*, 2010) and triggers ubiquitination and degradation of a mutant form of p53 (Parrales *et al.*, 2016). Thus, a given Hsp40 might either help protect or destroy different substrates—or have no effect—and different Hsp40s acting on a specific substrate might alternatively favor either ERAD or protein biogenesis (Meacham *et al.*, 1999; Farinha *et al.*, 2002; Zhang *et al.*, 2002; Schmidt *et al.*, 2009; Walker *et al.*, 2010; Park *et al.*, 2015; Parrales *et al.*, 2016). Related Hsp40s have also been found to bind in different ways to a given substrate (Irwin *et al.*, 2021). Similar phenomena have been observed for other chaperones (Brodsky, 2007; Preston and Brodsky, 2017). To date, there is no way to predict whether a chaperone will contribute to secretory protein folding or degradation.

The Hsp40 J domain stimulates the ATPase activity Hsp70 and uses a C-terminal region to bind substrates (Fan *et al.*, 2003; Craig and Marszalek, 2017). DNAJA1 is a class A Hsp40 that contains an N-terminal J domain of ~70 residues, a glycine phenylalanine-rich region (GF), and a zinc fingerlike region (ZFLR) that is followed by two structurally similar beta-barrel C-terminal domains (CTDs), CTD1 and CTD2, along with a dimerization domain (Qian *et al.*, 1996; Kityk *et al.*, 2018; Jiang *et al.*, 2019). The J domain forms a secondary structure harboring four alpha helices, and the highly conserved HPD tripeptide motif, situated between the second and third helices. This domain targets the Hsp70 nucleotide-binding domain, thereby enhancing its ATPase activity (Qian *et al.*, 1996; Kityk *et al.*, 2018; Jiang *et al.*, 2019). The ZFLR instead binds and aids in substrate folding (Lu and Cyr, 1998; Jiang *et al.*, 2019). The CTDs are responsible for substrate binding, yet recent studies emphasized the roles of other domains in substrate recognition (Kampinga and Craig, 2010; Yu *et al.*, 2015a,b; Schilke *et al.*, 2017). In contrast, class B Hsp40s lack the ZFLR and may present fewer binding interfaces for substrate association compared with class A Hsp40s. Moreover, a recent study reported that class B Hsp40s exhibit a unique autoinhibitory mechanism in which the Hsp70 binding sites are initially blocked by a short regulatory domain, but inhibition is released upon interaction with the Hsp70 C-terminal tail (Faust *et al.*, 2020). Together, differences in sequence and domain architecture between class A and class B Hsp40s expand substrate selectivity and specialization for Hsp70-dependent functions (Rebeaud *et al.*, 2021).

Since both DNAJA1 (this study) and Hsp70 (Gusarova *et al.*, 2001) associate with ApoB100, we hypothesize that DNAJA1 binds ApoB100 through the CTD(s). The Hsp40 might then recruit Hsp70 and stimulate Hsp70 activity via the J domain, thus coupling ApoB100 binding to ATP hydrolysis. In this scenario, DNAJA1 requires both the J domain and the CTD to regulate ApoB100 biogenesis. However, because Hsp40s act as homodimers and form intermolecular complexes with Hsp40s from another class via J domain-CTD1 salt bridges (Nillegoda *et al.*, 2015, 2017, 2018; Kirstein *et al.*, 2017), additional interaction sites might be available for substrate binding. As a consequence of ApoB100's size and multiple hydrophobic/lipid binding sites, it is also likely that several DNAJA1 molecules simultaneously associate with ApoB100. Further studies with DNAJA1 constructs harboring mutations in specific domains, along with studies involving truncated forms of ApoB100, will help determine which domains are necessary for chaperone-mediated regulation of ApoB100 during biogenesis in the ER.

Like DNAJA1, DNAJB1 is also an Hsp70 cochaperone (Michels *et al.*, 1999; Blard *et al.*, 2007; Gao *et al.*, 2015). In addition, DNAJB1 functions with mammalian Hsp110 and Hsp70 to disaggregate and refold luciferase aggregates and resolubilize alpha synuclein as well as tau aggregates (Hageman and Kampinga, 2009; Rampelt *et al.*, 2012; Kuo *et al.*, 2013; Mattoo *et al.*, 2013; Nillegoda *et al.*, 2015; Deane and Brown, 2017; Osaki *et al.*, 2018; den Brave *et al.*, 2020). Based on its role in stabilizing ApoB100, DNAJB1 might represent a therapeutic target since, in principle, its depletion would result in lower levels of circulating atherogenic lipoproteins. However, due to its participation in disaggregating toxic proteins, severe secondary effects would occur if DNAJB1 function was compromised. Nevertheless, it will be important to confirm the role of DNAJB1 in lipoprotein and cholesterol metabolism in vivo.

In sum, as overabundance of the atherogenic ApoB-containing particles is a major risk factor for CAD, a better understanding of the mechanism underlying the regulation of ApoB biogenesis may help offset the catastrophic effects of this disease. Drugs are in development that target many of the factors that impact ApoB100 biogenesis (Koishi *et al.*, 1992; Yokota *et al.*, 2000; Soti *et al.*, 2005; Assimon *et al.*, 2013; McConnell and McAlpine, 2013; Shevtsov *et al.*, 2019;

Lu *et al.*, 2020; Park *et al.*, 2020), some of which may also affect chaperone function. Thus, our work provides a necessary step toward the continued development of improved or complementary methods to treat CAD.

MATERIALS AND METHODS

Yeast strains, plasmids, and growth conditions

Yeast strains were grown at 30°C (unless otherwise indicated) using standard growth, media, and transformation conditions (Adams *et al.*, 1997). All the strains used in this study are listed in Supplemental Table S1. To drive expression of ApoB29, yeast were transformed with pSLW1-B29-HA (Hrizo *et al.*, 2007; Grubb *et al.*, 2012; Doonan *et al.*, 2019), which contains a *URA3* selection marker and encodes ApoB29 with a triple HA tag at the C-terminus. The ApoB29 isoform causes hypobetalipoproteinemia in humans but is the shortest isoform that can successfully traffic through the secretory pathway and is regulated by lipids (Collins *et al.*, 1988; Linton *et al.*, 1993; McLeod *et al.*, 1994). The expression of ApoB29 is under the control of a galactose inducible promoter, but because galactose is a nonoptimal carbon source and causes additional stress in yeast (Adams, 1972; Balch *et al.*, 2008), we used a β-estradiol inducible expression system driven by pACT1-GEV chimeric transcription factor.

To make yeast strains β-estradiol inducible, EcoRV (New England Biolabs) linearized pACT1-GEV plasmid was transformed into log phase yeast cells and integrated at the *leu2 Δ0* site using a standard lithium acetate protocol (Adams, 1972; Veatch *et al.*, 2009; McIsaac *et al.*, 2011; Doonan *et al.*, 2019). Transformants were selected on yeast peptone dextrose (YPD) plates containing 0.1 mg/ml nourseothricin (Werner Bioagents, Jena, Germany). To ensure selection of colonies with successful integration of the plasmid, positive colonies were restruck three times on YPD nourseothricin plates.

Yeast cycloheximide chase assays

Cycloheximide chase assays were conducted following published protocols (Hrizo *et al.*, 2007; Grubb *et al.*, 2012; Doonan *et al.*, 2019). In brief, to examine the rate of ApoB29 degradation, yeast transformed with pSLW1-B29-HA were grown overnight in synthetic media lacking uracil (SC-ura) supplemented with 2% glucose at 30°C and were then diluted with the same media and grown to logarithmic phase (OD_{600} = 0.4–0.6). Cells were harvested to obtain 1.0 OD_{600} equivalent of cells per time point and resuspended again in the same media but supplemented with 300 nM β-estradiol to induce expression of ApoB. All temperature-sensitive strains were preincubated at 37°C for 30 min. To inhibit protein translation, cycloheximide at a final concentration of 50 μg/ml was then added and 1.0 OD_{600} of cells was harvested as the 0-min time point. Equivalent amounts of cells were collected for the indicated subsequent time points. Total protein was precipitated using trichloroacetic acid (TCA) following published protocols and resolved by SDS–PAGE and quantitative Western blotting (Zhang *et al.*, 2001). The triple HA-tagged ApoB29 was detected using an anti-HA-horseradish peroxidase conjugated antibody, and G6PD levels were examined as a loading control with an anti-G6PD antibody (Supplemental Table S2).

Coimmunoprecipitation assays in yeast

To probe for specific protein–protein interactions, published protocols for ApoB29 in yeast were utilized (Hrizo *et al.*, 2007; Grubb *et al.*, 2012; Doonan *et al.*, 2019). In brief, yeast containing pSLW1-B29-HA were grown overnight at 30°C, the cells were diluted to 0.25 OD_{600}/ml, grown to an OD_{600} of 0.5, and 300 nM β-estradiol was added. Cell growth was continued for 2 h at 30°C. Once the OD_{600} reached 1.0, 100 OD_{600} of cells were harvested, which were then resuspended in 1 ml Roche lysis buffer (150 mM NaCl, 50 mM Tris-HCl, pH 7.5, 0.1% NP-40, 20 mM sodium molybdate, 1 mM phenylmethylsulfonyl fluoride [PMSF], 1 μg/ml leupeptin, 0.5 μg/ml pepstatin, and cOmplete EDTA-free protease inhibitor cocktail tablet [Millipore Sigma], hereafter referred to PIs + PIC for protease inhibitors and protease inhibitor cocktail).

Next, the cells were lysed using acid-washed mini glass beads by vigorous agitation on a Vortex mixer 3× for 2 min each with 2-min intervals on ice after each agitation. The lysate was collected and centrifuged for 2 min in a 4°C microcentrifuge at 5000 rpm, and the supernatant was transferred to a new microfuge tube and centrifugation was repeated. The cleared lysates were transferred to new tubes, 30 μl of a 1:1 slurry of Protein A Fast Flow–Sepharose beads (GE Healthcare) were added to each lysate, and tubes were placed on an end-to-end rotator for 1 h at 4°C. The tubes were centrifuged at 5000 rpm for 5 min at 4°C, the lysate was transferred to fresh tubes, and 5% (50 μl) of the initial volume was saved as input and processed by TCA precipitation as described earlier. The remaining lysate was diluted to 1.5 ml with Roche lysis buffer + PIs + PIC, 50 μl of anti HA affinity matrix (Roche) or an equal volume of Sepharose 6B beads (negative control) were added to the lysate, and the samples were placed on an end-to-end rotator at 4°C overnight. To isolate the bead-bound proteins, the lysates were centrifuged at 5000 rpm for 2 min at 4°C in a refrigerated microcentrifuge, and the supernatant (unbound fraction) was saved and stored at –80°C. The beads were then washed with 1 ml of ice-cold Roche lysis buffer + PIs+ PIC and again spun at 5000 rpm for 2 min at 4°C. This step was repeated twice, and two additional washes were conducted with the Roche lysis buffer containing PIs+ PIC but supplemented with 300 mM NaCl. After the final wash, any residual supernatant was removed, the beads were resuspended in 50 μl of TCA of sample buffer, and the solution was incubated at 37°C for 20 min and finally processed by SDS–PAGE and Western blotting. Proteins were detected using anti-HA, anti-ApoB, anti-Ydj1, anti-Ssa1, anti-PDI, anti-rpL5, anti-Sis1, and anti-G6PD antibody (see Supplemental Table S2).

Cell culture

McArdle RH-7777 cells (McArdle cells; ATCC CRL-1601) were purchased from American Type Culture Collection (ATCC) and grown at 37°C in a 5% CO_2 incubator in DMEM high glucose pyruvate (Thermo Scientific, Life Technologies) supplemented with 10% fetal bovine serum (FBS) (VWR), 10% horse serum (HS) (Sigma-Aldrich), and 0.1 mg/m penicillin/streptomycin (Thermo Fisher Scientific) on collagen-coated 10-ml dishes (Cellcoat Collagen Type I coated Petri dishes, Greiner). Cells were detached with 3 ml TrypLE Express Enzyme (No phenol Red, Life Technologies) for 3 min at 37°C. To quantify cell numbers, 40 μl of resuspended cells were mixed with 40 μl of trypan blue stain (Life Technologies) and an aliquot was analyzed on a hemocytometer. Cell culture experiments were performed in a 1300 Series A2 biosafety hood (Thermo Fisher Scientific).

Plasmids used in this study included HA-tagged ubiquitin (Kamitani *et al.*, 1997) and pcDNA3.1-CFTR (Han *et al.*, 2018). For transfection, 2×10^5 cells were seeded/well in 6-well collagen-coated plates (Greiner Bio-One), grown overnight, and treated with Lipofectamine 2000 following the manufacturer's instructions using Opti-MEM I reduced serum medium (Thermo Scientific Life Technologies) that was treated with 10 μl Lipofectamine 2000 and Opti-MEM I reduced serum medium (Thermo Scientific Life Technologies) with

4 µg of plasmid DNA. The solutions were then mixed and incubated for 20 min, and 500 µl of the mix were added to each well, followed by the addition of 2 ml of complete media. For transfection using 10-cm dishes, reagents were scaled up sixfold. Cells were harvested or lysed 20 h after transfection.

For knockdown studies, the siRNAs in Supplemental Table S3 were purchased from Dharmacon/Horizon Discovery. Initially, a set of four individual siRNAs (ON-TARGET plus Set of 4 Upgrade siRNA) was used to optimize knockdown conditions, followed by experiments using the most efficient siRNA. Lyophilized siRNAs were resuspended in nuclease free water to a final concentration of 20 µM. Knockdown efficiency was measured after 48 and 72 h and 20 and 30 nM of each siRNA were used. In all experiments, equal concentrations of fluorescent scrambled siRNA (BlockIt Alexa Fluor Red Fluorescent Control Oligo Invitrogen) were used.

Pulse-chase assays and measurements of ApoB100 ubiquitination

Pulse-chase assays were performed after modifications of published protocols (Bostrom *et al.*, 1986; Borchardt and Davis, 1987; Boren *et al.*, 1992, 1994; Fisher *et al.*, 1997; Gusarova *et al.*, 2001; Grubb *et al.*, 2012). McArdle cells (1×10^5) were seeded in 6-well collagen coated plates (see above) in 2 ml complete media and grown overnight. The cells were starved for 1 h in media lacking Cys/Met (DMEM) but containing L-Gln for 1 h at 37°C, washed with DPBS (Dulbecco phosphate-buffered saline), and then incubated in starvation media containing 100 mCi of S-35 (EasyTag Express 35-S Protein labeling mix; PerkinElmer) supplemented with 2% L-Gln. After 15 min, the cells were washed twice with DPBS and 1 ml of chase media (starvation media/2% Gln/5% FBS/5% HS/5%, 100 µM nonradioactive Cys, and 40 µM Met) was added to each well. Cells and media were collected at 15, 60, and 90 min into the chase. The media were collected into tubes with 25 µl of 1 mM PMSF. The cells were washed once with DPBS and lysed with 700 µl RadioIP assay buffer (RIPA) buffer (50 mM Tris-Cl, pH 7.4, 150 mM NaCl, 1% NP-40, 0.5% deoxycholate, 0.1% SDS, and PIs + PC) for 20–30 min on ice. The lysates were then centrifuged at $1600 \times g$ for 20 min in a microcentrifuge at 4°C, and the supernatant was collected. Radioactive counts were determined for each lysate and media sample in a scintillation counter, and immunoprecipitation reactions were set up (for each cellular lysate/well) with 680 µl DPBS, 120 µl 5× NET buffer (150 mM NaC1, 5 mM EDTA, and 50 mM Tris, pH 7.4, 0.5% Triton X-100, and 0.1% SDS), 5 µl of anti-ApoB antibody, 50 µl of a 1:1 Protein G bead slurry, 600 µl of lysate, and PIs + PIC. For the media samples, each immunoprecipitation contained 360 µl of double distilled water, 240 µl of 5× NET buffer, 5 µl of anti-ApoB antibody or anti-albumin antibody, 50 µl of a 1:1 Protein G bead slurry, 800 µl of sample, and PIs + PIC. After an overnight incubation at 4°C, the tubes were centrifuged at ~$1600 \times g$ for 1 min at 4°C in a microcentrifuge, and the beads were washed three times with 1× NET buffer with PIs + PIC. Next, the residual IP wash buffer was aspirated, and the beads were suspended in 75 µl urea sample buffer (8 M urea, 1% SDS, 10 mM EDTA, 150 mM Tris-Cl, pH 6.8). Proteins were resolved on 5% polyacrylamide SDS gels, and after the gels were dried and exposed to a phosphorimager screen, the radiograph was developed using a Typhoon FLA 7000 or Amersham Typhoon phosphorimager (GE Healthcare). Phosphorimages were collected at 50 µm resolution using a PMT voltage of 1000 V, and signals were quantified using ImageJ.

To measure the extent of protein ubiquitination, McArdle cells were transfected with an siRNA targeting the gene of interest, as described earlier, and on the next day cells were transfected with the HA-tagged ubiquitin expression plasmid (see above). After an overnight incubation, the media were aspirated, and fresh complete media with either the vehicle control (DMSO) or 25 mM of MG-132 (Selleck Chemicals) were added and the cells were incubated at 37°C for 1 h. Next, the media were aspirated and 500 µl of TrypLE were added. Following a 5-min incubation, the cells were harvested, and the cell pellets were lysed with 1 ml RIPA buffer + PIC supplemented with 25 µM MG-132 and 10 mM NEM for 20–30 min on ice. After centrifugation at ~$1600 \times g$ for 20 min at 4°, the supernatant was collected and precleared with 30 µl of a 1:1 slurry of Protein G–Sepharose (GE Healthcare 17061801) beads for 1 h at 4°C. The cleared lysate was then collected after a ~$1000 \times g$ spin for 5 min at 4°C, and protein levels were normalized using a BCA assay (ThermoScientific) following the manufacturer's instructions. A fraction (20%) of the total lysate was saved for each reaction as the input, and equal amounts of protein plus 120 µl 1× NET buffer and 100 µl DPBS (Life Technologies) including PIC, 25 µM MG-132, and 50 µl of a 1:1 slurry of Protein G–Sepharose (GE Healthcare) and 3 µl anti-ApoB antibody (Calbiochem) were added to each immunoprecipitation. The tubes were incubated at 4°C overnight, centrifuged at ~$1600 \times g$ for 1 min at 4°C, and washed three times with 1× NET including PIs + PIC, and the beads were suspended in urea sample buffer. Proteins were resolved on 5% polyacrylamide SDS gels, and ubiquitinated ApoB was detected with HA-HRP conjugated antibody. Another set of blots was probed with anti-ApoB antibody.

Other biochemical methods

To perform chemical cross-linking in McArdle cells, 1×10^6 cells were seeded in 10-cm dishes in 10 ml and grown overnight, as above. The cells were washed twice with DPBS, and 2 mM DSP (ThermoFisher) was added at room temperature for 30 min. Next, stop solution (20 mM Tris-Cl, pH 7.5) was added and the cells were incubated for another 15 min before the cells were trypsinized and isolated as above. The cells were lysed in RIPA buffer, and immunoprecipitation reactions were set up as described for the pulse-chase protocol. To cleave DSP, 75 µl of urea sample buffer supplemented with 50 mM of freshly prepared DTT was added to each sample, which was then incubated at 37°C for 30 min.

Sucrose gradient analysis of ApoB-containing lipoproteins was conducted following published protocols (Boren *et al.*, 1992, 1994) using cells that were seeded at 6×10^5 cells/well and grown overnight in complete medium. The next day, siRNA transfections were performed, as above, and after 48 h, a pulse-chase was conducted as described above. However, media were collected only at the 90-min time point. Next, a gradient was set up with 2 ml of 50 and 25% (wt/vol) sucrose onto which the isolated media containing identical amounts of radioactivity diluted to 12.5% (wt/vol) sucrose concentration in a total volume of 5 ml was loaded. Each solution also contained 50 mM Na_3PO_4, pH 7.4, 150 mM NaCl, 5 mM EDTA, and PIs + PIC. Finally, 3 ml of media were layered on top. After centrifugation in a SW Ti41 rotor in a Beckman LM centrifuge at $150{,}000 \times g$ for 65 h at 4°C, 12 1-ml fractions were carefully collected from the top, and radioactivity and the refractive index of each fraction were calculated using a scintillation counter and an Abbe refractometer, respectively. Next, an overnight immunoprecipitation with anti-ApoB antibody and Protein G beads as performed, as outlined above. Samples were subjected to SDS–PAGE, and the gels were dried and exposed to a phosphorimager screen, which was developed using a Typhoon FLA 7000 or Amersham Typhoon phosphorimager (GE Healthcare). Phosphorimages were collected at

50 µm resolution using PMT voltage of 1000 V, and the signal was quantified using ImageJ.

To assay ApoB100 solubility in various detergents, cells were grown overnight and siRNA-mediated DNAJA1 knockdown was conducted as described above. Scrambled control and DNAJA1-depleted cells were incubated with the indicated concentrations of dodecyl D-maltoside (DDM) (Sigma Aldrich) in 0.3 M sucrose, 0.1 M KCl, 2.5 mM $MgCl_2$,1 mM sodium-free EDTA, 10 mM PIPES, pH 6.8, and PIs + PIC on ice for 20 min. After centrifugation at 100,000 × *g* at 4°C for 1 h, the soluble (supernatant) and insoluble (pellet) fractions were processed for SDS–PAGE and developed by Western blot analysis with anti-ApoB antibody. The levels of DNAJA1 were also examined with DNAJA1 antibody, and ribophorin was used as a control (Crimaudo *et al.*, 1987).

Indirect immunofluorescence (IF)

McArdle cells were grown on fibronectin-coated coverslips and transfected with scrambled siRNA (control) or an siRNA targeting DNAJA1, as described above. After 48 h, cells were fixed with 4% paraformaldehyde solution and then incubated with primary antibodies against ApoB (1:100; Santa Cruz Biotechnology 393636) and HMGCR (1:100; Biorbyt orb340767) at 4°C overnight. Cells were then washed with 1% bovine serum albumin solution and incubated with Alexa dye conjugated secondary antibodies for 1 h in the dark. Mounting solution containing DAPI was used to label the nucleus. Images were taken on a Nikon A1R confocal microscope with 60× objective and analyzed with Fuji software (National Institutes of Health ([NIH]).

Materials, quantification, and statistical analysis

The commercial sources and catalogue numbers for other purchased reagents are listed in Supplemental Table S4.

For quantitative Western blots, proteins were visualized using SuperSignal West Pico or the Femto Chemiluminescent kit (ThermoFisher) along with the respective Pro-Signal Pico or Femto developer solutions (Prometheus) using a Bio-Rad universal Hood II Imager. Image J software (NIH) were used to obtain and quantify images. Sample size comprised the stated number of independent biological replicates that individually also included three to four technical replicates. Statistical significance was calculated by Student's unpaired *t* tests using the GraphPad statistical software.

For pulse-chase experiments, samples were normalized based on radioactive counts, and the signal after phosphorimager analysis (see above) was quantified using ImageJ (NIH). Radiographs were saved as TIFF files (8/16 bit) to collect raw integrated densities. Student's unpaired two-tailed *t* tests were performed on GraphPad, average and standard errors were calculated, and significance was determined. Independent experiments were biological replicates which included the average of two to three technical replicates. For ubiquitination assays, data were normalized to the corresponding ApoB100 levels. Statistical significance was again determined by conducting unpaired *t* tests via the GraphPad statistical software.

ACKNOWLEDGMENTS

This work was supported by NIH Grant HL127930 (to E.A.F. and J.L.B.) and Grant GM131732 (to J.L.B.). D.K. acknowledges support from an American Heart Association predoctoral fellowship (19PRE34380412). We thank Grant Daskivich, Vlad Denic, Lynley Doonan, Sam Estabrooks, Arjun Mittal, Cyrus Nikain, Sara Sannino, Randy Schekman, and Haizhen Wang for reagents and advice.

REFERENCES

Abisambra JF, Jinwal UK, Suntharalingam A, Arulselvam K, Brady S, Cockman M, Jin Y, Zhang B, Dickey CA (2012). DnaJA1 antagonizes constitutive Hsp70-mediated stabilization of tau. J Mol Biol 421, 653–661.

Adams A, Gottschling DE, Kaiser CA, Stearns T (1997). Methods in Yeast Genetics: A Cold Spring Harbor Laboratory Course Manual, Cold Spring Harbor, NY: Cold Spring Harbor Laboratory Press.

Adams BG (1972). Induction of galactokinase in Saccharomyces cerevisiae: kinetics of induction and glucose effects. J Bacteriol 111, 308–315.

Adhyaru BB, Jacobson TA (2018). Safety and efficacy of statin therapy. Nat Rev Cardiol 15, 757–769.

Assimon VA, Gillies AT, Rauch JN, Gestwicki JE (2013). Hsp70 protein complexes as drug targets. Curr Pharm Des 19, 404–417.

Astaneh B, Makhdami N, Astaneh V, Guyatt G (2021). The effect of mipomersen in the management of patients with familial hypercholesterolemia: a systematic review and meta-analysis of clinical trials. J Cardiovasc Dev Dis 8. 10.3390/jcdd8070082.

Balch WE, Morimoto RI, Dillin A, Kelly JW (2008). Adapting proteostasis for disease intervention. Science 319, 916–919.

Becker J, Walter W, Yan W, Craig EA (1996). Functional interaction of cytosolic hsp70 and a DnaJ-related protein, Ydj1p, in protein translocation in vivo. Mol Cell Biol 16, 4378–4386.

Beilharz T, Egan B, Silver PA, Hofmann K, Lithgow T (2003). Bipartite signals mediate subcellular targeting of tail-anchored membrane proteins in Saccharomyces cerevisiae. J Biol Chem 278, 8219–8223.

Benjamin EJ, Muntner P, Alonso A, Bittencourt MS, Callaway CW, Carson AP, Chamberlain AM, Chang AR, Cheng S, Das SR, *et al.* (2019). Heart disease and stroke statistics—2019 update: A report from the American Heart Association. Circulation 139, e56–e528.

Benoist F, Grand-Perret T (1997). Co-translational degradation of apolipoprotein B100 by the proteasome is prevented by microsomal triglyceride transfer protein. Synchronized translation studies on HepG2 cells treated with an inhibitor of microsomal triglyceride transfer protein. J Biol Chem 272, 20435–20442.

Blard O, Feuillette S, Bou J, Chaumette B, Frebourg T, Campion D, Lecourtois M (2007). Cytoskeleton proteins are modulators of mutant tau-induced neurodegeneration in Drosophila. Hum Mol Genet 16, 555–566.

Boekholdt SM, Hovingh GK, Mora S, Arsenault BJ, Amarenco P, Pedersen TR, LaRosa JC, Waters DD, DeMicco DA, Simes RJ, *et al.* (2014). Very low levels of atherogenic lipoproteins and the risk for cardiovascular events: a meta-analysis of statin trials. J Am Coll Cardiol 64, 485–494.

Borchardt RA, Davis RA (1987). Intrahepatic assembly of very low density lipoproteins. Rate of transport out of the endoplasmic reticulum determines rate of secretion. J Biol Chem 262, 16394–16402.

Boren J, Graham L, Wettesten M, Scott J, White A, Olofsson SO (1992). The assembly and secretion of ApoB 100-containing lipoproteins in Hep G2 cells. ApoB 100 is cotranslationally integrated into lipoproteins. J Biol Chem 267, 9858–9867.

Boren J, Rustaeus S, Olofsson SO (1994). Studies on the assembly of apolipoprotein B-100- and B-48-containing very low density lipoproteins in McA-RH7777 cells. J Biol Chem 269, 25879–25888.

Bostrom K, Wettesten M, Boren J, Bondjers G, Wiklund O, Olofsson SO (1986). Pulse-chase studies of the synthesis and intracellular transport of apolipoprotein B-100 in Hep G2 cells. J Biol Chem 261, 13800–13806.

Brodsky JL (2007). The protective and destructive roles played by molecular chaperones during ERAD (endoplasmic-reticulum-associated degradation). Biochem J 404, 353–363.

Brodsky JL, Fisher EA (2008). The many intersecting pathways underlying apolipoprotein B secretion and degradation. Trends Endocrinol Metab 19, 254–259.

Butkinaree C, Guo L, Ramkhelawon B, Wanschel A, Brodsky JL, Moore KJ, Fisher EA (2014). A regulator of secretory vesicle size, Kelch-like protein 12, facilitates the secretion of apolipoprotein B100 and very-low-density lipoproteins–brief report. Arterioscler Thromb Vasc Biol 34, 251–254.

Calcutta A, Jessen CM, Behrens MA, Oliveira CL, Renart ML, Gonzalez-Ros JM, Otzen DE, Pedersen JS, Malmendal A, Nielsen NC (2012). Mapping of unfolding states of integral helical membrane proteins by GPS-NMR and scattering techniques: TFE-induced unfolding of KcsA in DDM surfactant. Biochim Biophys Acta 1818, 2290–2301.

Caplan AJ, Douglas MG (1991). Characterization of YDJ1: a yeast homologue of the bacterial dnaJ protein. J Cell Biol 114, 609–621.

Cardozo C, Wu X, Pan M, Wang H, Fisher EA (2002). The inhibition of microsomal triglyceride transfer protein activity in rat hepatoma cells

promotes proteasomal and nonproteasomal degradation of apoprotein b100. Biochemistry 41, 10105–10114.
Chen PF, Marcel YL, Yang CY, Gotto AM Jr, Milne RW, Sparrow JT, Chan L (1988). Primary sequence mapping of human apolipoprotein B-100 epitopes. Comparisons of trypsin accessibility and immunoreactivity and implication for apoB conformation. Eur J Biochem 175, 111–118.
Chen SH, Habib G, Yang CY, Gu ZW, Lee BR, Weng SA, Silberman SR, Cai SJ, Deslypere JP, Rosseneu M, *et al*. (1987). Apolipoprotein B-48 is the product of a messenger RNA with an organ-specific in-frame stop codon. Science 238, 363–366.
Chen SH, Yang CY, Chen PF, Setzer D, Tanimura M, Li WH, Gotto AM Jr, Chan L (1986). The complete cDNA and amino acid sequence of human apolipoprotein B-100. J Biol Chem 261, 12918–12921.
Chen Y, Le Caherec F, Chuck SL (1998). Calnexin and other factors that alter translocation affect the rapid binding of ubiquitin to apoB in the Sec61 complex. J Biol Chem 273, 11887–11894.
Collins DR, Knott TJ, Pease RJ, Powell LM, Wallis SC, Robertson S, Pullinger CR, Milne RW, Marcel YL, Humphries SE, *et al*. (1988). Truncated variants of apolipoprotein B cause hypobetalipoproteinaemia. Nucleic Acids Res 16, 8361–8375.
Costanzo MC, Crawford ME, Hirschman JE, Kranz JE, Olsen P, Robertson LS, Skrzypek MS, Braun BR, Hopkins KL, Kondu P, *et al*. (2001). YPD, PombePD and WormPD: model organism volumes of the BioKnowledge library, an integrated resource for protein information. Nucleic Acids Res 29, 75–79.
Craig EA, Marszalek J (2017). How do J-proteins get Hsp70 to do so many different things? Trends Biochem Sci 42, 355–368.
Crimaudo C, Hortsch M, Gausepohl H, Meyer DI (1987). Human ribophorins I and II: the primary structure and membrane topology of two highly conserved rough endoplasmic reticulum-specific glycoproteins. EMBO J 6, 75–82.
Cyr DM, Douglas MG (1994). Differential regulation of Hsp70 subfamilies by the eukaryotic DnaJ homologue YDJ1. J Biol Chem 269, 9798–9804.
Cyr DM, Lu X, Douglas MG (1992). Regulation of Hsp70 function by a eukaryotic DnaJ homolog. J Biol Chem 267, 20927–20931.
Dadu RT, Ballantyne CM (2014). Lipid lowering with PCSK9 inhibitors. Nat Rev Cardiol 11, 563–575.
De Mattos EP, Wentink A, Nussbaum-Krammer C, Hansen C, Bergink S, Melki R, Kampinga HH (2020). Protein quality control pathways at the crossroad of synucleinopathies. J Parkinsons Dis 10, 369–382.
Deane CA, Brown IR (2017). Components of a mammalian protein disaggregation/refolding machine are targeted to nuclear speckles following thermal stress in differentiated human neuronal cells. Cell Stress Chaperones 22, 191–200.
Dekker SL, Kampinga HH, Bergink S (2015). DNAJs: more than substrate delivery to HSPA. Front Mol Biosci 2, 35.
den Brave F, Cairo LV, Jagadeesan C, Ruger-Herreros C, Mogk A, Bukau B, Jentsch S (2020). Chaperone-mediated protein disaggregation triggers proteolytic clearance of intra-nuclear protein inclusions. Cell Rep 31, 107680.
Doonan LM, Guerriero CJ, Preston GM, Buck TM, Khazanov N, Fisher EA, Senderowitz H, Brodsky JL (2019). Hsp104 facilitates the endoplasmic-reticulum-associated degradation of disease-associated and aggregation-prone substrates. Protein Sci 28, 1290–1306.
Estabrooks S, Brodsky JL (2020). Regulation of CFTR biogenesis by the proteostatic network and pharmacological modulators. Int J Mol Sci 21. 10.3390/ijms21020452.
Fan CY, Lee S, Cyr DM (2003). Mechanisms for regulation of Hsp70 function by Hsp40. Cell Stress Chaperones 8, 309–316.
Farinha CM, Nogueira P, Mendes F, Penque D, Amaral MD (2002). The human DnaJ homologue (Hdj)-1/heat-shock protein (Hsp) 40 co-chaperone is required for the in vivo stabilization of the cystic fibrosis transmembrane conductance regulator by Hsp70. Biochem J 366, 797–806.
Faust O, Abayev-Avraham M, Wentink AS, Maurer M, Nillegoda NB, London N, Bukau B, Rosenzweig R (2020). HSP40 proteins use class-specific regulation to drive HSP70 functional diversity. Nature 587, 489–494.
Fisher EA, Khanna NA, McLeod RS (2011). Ubiquitination regulates the assembly of VLDL in HepG2 cells and is the committing step of the apoB-100 ERAD pathway. J Lipid Res 52, 1170–1180.
Fisher EA, Lapierre LR, Junkins RD, McLeod RS (2008). The AAA-ATPase p97 facilitates degradation of apolipoprotein B by the ubiquitin-proteasome pathway. J Lipid Res 49, 2149–2160.
Fisher EA, Zhou M, Mitchell DM, Wu X, Omura S, Wang H, Goldberg AL, Ginsberg HN (1997). The degradation of apolipoprotein B100 is mediated by the ubiquitin-proteasome pathway and involves heat shock protein 70. J Biol Chem 272, 20427–20434.
Gao X, Carroni M, Nussbaum-Krammer C, Mogk A, Nillegoda NB, Szlachcic A, Guilbride DL, Saibil HR, Mayer MP, Bukau B (2015). Human Hsp70 disaggregase reverses Parkinson's-linked alpha-synuclein amyloid fibrils. Mol Cell 59, 781–793.
Ginsberg HN (1997). Role of lipid synthesis, chaperone proteins and proteasomes in the assembly and secretion of apoprotein B-containing lipoproteins from cultured liver cells. Clin Exp Pharmacol Physiol 24, A29–A32.
Glover JR, Lindquist S (1998). Hsp104, Hsp70, and Hsp40: a novel chaperone system that rescues previously aggregated proteins. Cell 94, 73–82.
Goldstein JL, Brown MS (2015). A century of cholesterol and coronaries: from plaques to genes to statins. Cell 161, 161–172.
Gordon DA, Jamil H, Gregg RE, Olofsson SO, Boren J (1996). Inhibition of the microsomal triglyceride transfer protein blocks the first step of apolipoprotein B lipoprotein assembly but not the addition of bulk core lipids in the second step. J Biol Chem 271, 33047–33053.
Grubb S, Guo L, Fisher EA, Brodsky JL (2012). Protein disulfide isomerases contribute differentially to the endoplasmic reticulum-associated degradation of apolipoprotein B and other substrates. Mol Biol Cell 23, 520–532.
Gusarova V, Brodsky JL, Fisher EA (2003). Apolipoprotein B100 exit from the endoplasmic reticulum (ER) is COPII-dependent, and its lipidation to very low density lipoprotein occurs post-ER. J Biol Chem 278, 48051–48058.
Gusarova V, Caplan AJ, Brodsky JL, Fisher EA (2001). Apoprotein B degradation is promoted by the molecular chaperones hsp90 and hsp70. J Biol Chem 276, 24891–24900.
Hageman J, Kampinga HH (2009). Computational analysis of the human HSPH/HSPA/DNAJ family and cloning of a human HSPH/HSPA/DNAJ expression library. Cell Stress Chaperones 14, 1–21.
Han ST, Rab A, Pellicore MJ, Davis EF, McCague AF, Evans TA, Joynt AT, Lu Z, Cai Z, Raraigh KS, *et al*. (2018). Residual function of cystic fibrosis mutants predicts response to small molecule CFTR modulators. JCI Insight 3. 10.1172/jci.insight.121159.
Heinemeyer T, Stemmet M, Bardien S, Neethling A (2019). Underappreciated roles of the translocase of the outer and inner mitochondrial membrane protein complexes in human disease. DNA Cell Biol 38, 23–40.
Heron M (2017). Deaths: Leading causes for 2015. Natl Vital Stat Rep 66, 1–76.
Hoe KL, Won M, Chung KS, Jang YJ, Lee SB, Kim DU, Lee JW, Yun JH, Yoo HS (1998). Isolation of a new member of DnaJ-like heat shock protein 40 (Hsp40) from human liver. Biochim Biophys Acta 1383, 4–8.
Hrizo SL, Gusarova V, Habiel DM, Goeckeler JL, Fisher EA, Brodsky JL (2007). The Hsp110 molecular chaperone stabilizes apolipoprotein B from endoplasmic reticulum-associated degradation (ERAD). J Biol Chem 282, 32665–32675.
Hussain MM, Fatma S, Pan X, Iqbal J (2005). Intestinal lipoprotein assembly. Curr Opin Lipidol 16, 281–285.
Hussain MM, Kancha RK, Zhou Z, Luchoomun J, Zu H, Bakillah A (1996). Chylomicron assembly and catabolism: role of apolipoproteins and receptors. Biochim Biophys Acta 1300, 151–170.
Irwin R, Faust O, Petrovic I, Wolf SG, Hofmann H, Rosenzweig R (2021). Hsp40s play complementary roles in the prevention of tau amyloid formation. Elife 10. 10.7554/eLife.69601.
Jang AY, Han SH, Sohn IS, Oh PC, Koh KK (2020). Lipoprotein(a) and cardiovascular diseases—revisited. Circ J. 10.1253/circj.CJ-20-0051.
Janz A, Chen R, Regensburger M, Ueda Y, Rost S, Klopocki E, Gunther K, Edenhofer F, Duff HJ, Ergun S, Gerull B (2020). Generation of two patient-derived iPSC lines from siblings (LIBUCi001-A and LIBUCi002-A) and a genetically modified iPSC line (JMUi001-A-1) to mimic dilated cardiomyopathy with ataxia (DCMA) caused by a homozygous DNAJC19 mutation. Stem Cell Res 46, 101856.
Jiang Y, Rossi P, Kalodimos CG (2019). Structural basis for client recognition and activity of Hsp40 chaperones. Science 365, 1313–1319.
Kamitani T, Kito K, Nguyen HP, Yeh ET (1997). Characterization of NEDD8, a developmentally down-regulated ubiquitin-like protein. J Biol Chem 272, 28557–28562.
Kampinga HH, Andreasson C, Barducci A, Cheetham ME, Cyr D, Emanuelsson C, Genevaux P, Gestwicki JE, Goloubinoff P, Huerta-Cepas J, *et al*. (2019). Function, evolution, and structure of J-domain proteins. Cell Stress Chaperones 24, 7–15.
Kampinga HH, Craig EA (2010). The HSP70 chaperone machinery: J proteins as drivers of functional specificity. Nat Rev Mol Cell Biol 11, 579–592.
Kirstein J, Arnsburg K, Scior A, Szlachcic A, Guilbride DL, Morimoto RI, Bukau B, Nillegoda NB (2017). In vivo properties of the disaggregase

function of J-proteins and Hsc70 in Caenorhabditis elegans stress and aging. Aging Cell 16, 1414–1424.
Kityk R, Kopp J, Mayer MP (2018). Molecular Mechanism of J-Domain-Triggered ATP Hydrolysis by Hsp70 Chaperones. Mol Cell 69, 227–237 e224.
Koishi M, Hosokawa N, Sato M, Nakai A, Hirayoshi K, Hiraoka M, Abe M, Nagata K (1992). Quercetin, an inhibitor of heat shock protein synthesis, inhibits the acquisition of thermotolerance in a human colon carcinoma cell line. Jpn J Cancer Res 83, 1216–1222.
Kuo Y, Ren S, Lao U, Edgar BA, Wang T (2013). Suppression of polyglutamine protein toxicity by co-expression of a heat-shock protein 40 and a heat-shock protein 110. Cell Death Dis 4, e833.
Larsen LE, Stoekenbroek RM, Kastelein JJP, Holleboom AG (2019). Moving targets: Recent advances in lipid-lowering therapies. Arterioscler Thromb Vasc Biol 39, 349–359.
Liang JS, Kim T, Fang S, Yamaguchi J, Weissman AM, Fisher EA, Ginsberg HN (2003a). Overexpression of the tumor autocrine motility factor receptor Gp78, a ubiquitin protein ligase, results in increased ubiquitinylation and decreased secretion of apolipoprotein B100 in HepG2 cells. J Biol Chem 278, 23984–23988.
Liang JS, Kim T, Fang S, Yamaguchi J, Weissman AM, Fisher EA, Ginsberg HN (2003b). Overexpression of the tumor autocrine motility factor receptor Gp78, a ubiquitin protein ligase, results in increased ubiquitinylation and decreased secretion of apolipoprotein B100 in HepG2 cells. J Biol Chem 278, 23984–23988.
Liang S, Wu X, Fisher EA, Ginsberg HN (2000). The amino-terminal domain of apolipoprotein B does not undergo retrograde translocation from the endoplasmic reticulum to the cytosol. Proteasomal degradation of nascent apolipoprotein B begins at the carboxyl terminus of the protein, while apolipoprotein B is still in its original translocon. J Biol Chem 275, 32003–32010.
Libby P, Everett BM (2019). Novel antiatherosclerotic therapies. Arterioscler Thromb Vasc Biol 39, 538–545.
Linton MF, Farese RV Jr, Young SG. (1993). Familial hypobetalipoproteinemia. J Lipid Res 34, 521–541.
Liu Q, Liang C, Zhou L (2020). Structural and functional analysis of the Hsp70/Hsp40 chaperone system. Protein Sci 29, 378–390.
Lu H, Zhou Q, He J, Jiang Z, Peng C, Tong R, Shi J (2020). Recent advances in the development of protein-protein interactions modulators: mechanisms and clinical trials. Signal Transduct Target Ther 5, 213.
Lu Z, Cyr DM (1998). The conserved carboxyl terminus and zinc finger-like domain of the co-chaperone Ydj1 assist Hsp70 in protein folding. J Biol Chem 273, 5970–5978.
Mattoo RUH, Sharma SK, Priya S, Finka A, Goloubinoff P (2013). Hsp110 is a bona fide chaperone using ATP to unfold stable misfolded polypeptides and reciprocally collaborate with Hsp70 to solubilize protein aggregates. J Biol Chem 288, 21399–21411.
Mattson G, Conklin E, Desai S, Nielander G, Savage MD, Morgensen S (1993). A practical approach to crosslinking. Mol Biol Rep 17, 167–183.
McConnell JR, McAlpine SR (2013). Heat shock proteins 27, 40, and 70 as combinational and dual therapeutic cancer targets. Bioorg Med Chem Lett 23, 1923–1928.
McIsaac RS, Silverman SJ, McClean MN, Gibney PA, Macinskas J, Hickman MJ, Petti AA, Botstein D (2011). Fast-acting and nearly gratuitous induction of gene expression and protein depletion in Saccharomyces cerevisiae. Mol Biol Cell 22, 4447–4459.
McLeod RS, Zhao Y, Selby SL, Westerlund J, Yao Z (1994). Carboxyl-terminal truncation impairs lipid recruitment by apolipoprotein B100 but does not affect secretion of the truncated apolipoprotein B-containing lipoproteins. J Biol Chem 269, 2852–2862.
Meacham GC, Lu Z, King S, Sorscher E, Tousson A, Cyr DM (1999). The Hdj-2/Hsc70 chaperone pair facilitates early steps in CFTR biogenesis. EMBO J 18, 1492–1505.
Meex SJ, Andreo U, Sparks JD, Fisher EA (2011). Huh-7 or HepG2 cells: which is the better model for studying human apolipoprotein-B100 assembly and secretion? J Lipid Res 52, 152–158.
Meshalkina DA, Shevtsov MA, Dobrodumov AV, Komarova EY, Voronkina IV, Lazarev VF, Margulis BA, Guzhova IV (2016). Knock-down of Hdj2/DNAJA1 co-chaperone results in an unexpected burst of tumorigenicity of C6 glioblastoma cells. Oncotarget 7, 22050–22063.
Michels AA, Kanon B, Bensaude O, Kampinga HH (1999). Heat shock protein (Hsp) 40 mutants inhibit Hsp70 in mammalian cells. J Biol Chem 274, 36757–36763.
Mitchell DM, Zhou M, Pariyarath R, Wang H, Aitchison JD, Ginsberg HN, Fisher EA (1998). Apoprotein B100 has a prolonged interaction with the translocon during which its lipidation and translocation change from dependence on the microsomal triglyceride transfer protein to independence. Proc Natl Acad Sci USA 95, 14733–14738.
Nakatsukasa K, Huyer G, Michaelis S, Brodsky JL (2008). Dissecting the ER-associated degradation of a misfolded polytopic membrane protein. Cell 132, 101–112.
Nandakumar R, Matveyenko A, Thomas T, Pavlyha M, Ngai C, Holleran S, Ramakrishnan R, Ginsberg HN, Karmally W, Marcovina SM, Reyes-Soffer G (2018). Effects of mipomersen, an apolipoprotein B100 antisense, on lipoprotein (a) metabolism in healthy subjects. J Lipid Res 59, 2397–2402.
Nillegoda NB, Kirstein J, Szlachcic A, Berynskyy M, Stank A, Stengel F, Arnsburg K, Gao X, Scior A, Aebersold R, *et al.* (2015). Crucial HSP70 co-chaperone complex unlocks metazoan protein disaggregation. Nature 524, 247–251.
Nillegoda NB, Stank A, Malinverni D, Alberts N, Szlachcic A, Barducci A, De Los Rios P, Wade RC, Bukau B (2017). Evolution of an intricate J-protein network driving protein disaggregation in eukaryotes. Elife 6. 10.7554/eLife.24560.
Nillegoda NB, Wentink AS, Bukau B (2018). Protein disaggregation in multicellular organisms. Trends Biochem Sci 43, 285–300.
Okiyoneda T, Apaja PM, Lukacs GL (2011). Protein quality control at the plasma membrane. Curr Opin Cell Biol 23, 483–491.
Olofsson SO, Bjursell G, Bostrom K, Carlsson P, Elovson J, Protter AA, Reuben MA, Bondjers G (1987). Apolipoprotein B: structure, biosynthesis and role in the lipoprotein assembly process. Atherosclerosis 68, 1–17.
Osaki Y, Saito A, Kanemoto S, Kaneko M, Matsuhisa K, Asada R, Masaki T, Orii K, Fukao T, Tomatsu S, Imaizumi K (2018). Shutdown of ER-associated degradation pathway rescues functions of mutant iduronate 2-sulfatase linked to mucopolysaccharidosis type II. Cell Death Dis 9, 808.
Oyadomari S, Yun C, Fisher EA, Kreglinger N, Kreibich G, Oyadomari M, Harding HP, Goodman AG, Harant H, Garrison JL, *et al.* (2006). Cotranslocational degradation protects the stressed endoplasmic reticulum from protein overload. Cell 126, 727–739.
Park HK, Yoon NG, Lee JE, Hu S, Yoon S, Kim SY, Hong JH, Nam D, Chae YC, Park JB, Kang BH (2020). Unleashing the full potential of Hsp90 inhibitors as cancer therapeutics through simultaneous inactivation of Hsp90, Grp94, and TRAP1. Exp Mol Med 52, 79–91.
Park SY, Choi HK, Seo JS, Yoo JY, Jeong JW, Choi Y, Choi KC, Yoon HG (2015). DNAJB1 negatively regulates MIG6 to promote epidermal growth factor receptor signaling. Biochim Biophys Acta 1853, 2722–2730.
Parrales A, Ranjan A, Iyer SV, Padhye S, Weir SJ, Roy A, Iwakuma T (2016). DNAJA1 controls the fate of misfolded mutant p53 through the mevalonate pathway. Nat Cell Biol 18, 1233–1243.
Parsell DA, Kowal AS, Singer MA, Lindquist S (1994). Protein disaggregation mediated by heat-shock protein Hsp104. Nature 372, 475–478.
Powell LM, Wallis SC, Pease RJ, Edwards YH, Knott TJ, Scott J (1987). A novel form of tissue-specific RNA processing produces apolipoprotein-B48 in intestine. Cell 50, 831–840.
Preston GM, Brodsky JL (2017). The evolving role of ubiquitin modification in endoplasmic reticulum-associated degradation. Biochem J 474, 445–469.
Preston GM, Guerriero CJ, Metzger MB, Michaelis S, Brodsky JL (2018). Substrate insolubility dictates Hsp104-dependent endoplasmic-reticulum-associated degradation. Mol Cell 70, 242–253.e246.
Qian YQ, Patel D, Hartl FU, McColl DJ (1996). Nuclear magnetic resonance solution structure of the human Hsp40 (HDJ-1) J-domain. J Mol Biol 260, 224–235.
Rampelt H, Kirstein-Miles J, Nillegoda NB, Chi K, Scholz SR, Morimoto RI, Bukau B (2012). Metazoan Hsp70 machines use Hsp110 to power protein disaggregation. EMBO J 31, 4221–4235.
Rauch JN, Gestwicki JE (2014). Binding of human nucleotide exchange factors to heat shock protein 70 (Hsp70) generates functionally distinct complexes in vitro. J Biol Chem 289, 1402–1414.
Rebeaud ME, Mallik S, Goloubinoff P, Tawfik DS (2021). On the evolution of chaperones and cochaperones and the expansion of proteomes across the Tree of Life. Proc Natl Acad Sci USA 118. 10.1073/pnas.2020885118.
Reiner Z (2014). Resistance and intolerance to statins. Nutr Metab Cardiovasc Dis 24, 1057–1066.
Reiner Z, De Bacquer D, Kotseva K, Prugger C, De Backer G, Wood D, Group EIS (2013). Treatment potential for dyslipidaemia management in patients with coronary heart disease across Europe: findings from the EUROASPIRE III survey. Atherosclerosis 231, 300–307.
Reiner Z, Tedeschi-Reiner E (2013). Prevalence and types of persistent dyslipidemia in patients treated with statins. Croat Med J 54, 339–345.

Reyes-Soffer G, Moon B, Hernandez-Ono A, Dionizovik-Dimanovski M, Jimenez J, Obunike J, Thomas T, Ngai C, Fontanez N, Donovan DS, *et al*. (2016). Complex effects of inhibiting hepatic apolipoprotein B100 synthesis in humans. Sci Transl Med 8, 323ra312.
Rutkowski DT, Kang SW, Goodman AG, Garrison JL, Taunton J, Katze MG, Kaufman RJ, Hegde RS (2007). The role of p58IPK in protecting the stressed endoplasmic reticulum. Mol Biol Cell 18, 3681–3691.
Rutledge AC, Qiu W, Zhang R, Kohen-Avramoglu R, Nemat-Gorgani N, Adeli K (2009). Mechanisms targeting apolipoprotein B100 to proteasomal degradation: evidence that degradation is initiated by BiP binding at the N terminus and the formation of a p97 complex at the C terminus. Arterioscler Thromb Vasc Biol 29, 579–585.
Rutledge AC, Qiu W, Zhang R, Urade R, Adeli K (2013). Role of cysteine-protease CGHC motifs of ER-60, a protein disulfide isomerase, in hepatic apolipoprotein B100 degradation. Arch Biochem Biophys 537, 104–112.
Sahi C, Craig EA (2007). Network of general and specialty J protein chaperones of the yeast cytosol. Proc Natl Acad Sci USA 104, 7163–7168.
Sakata N, Stoops JD, Dixon JL (1999). Cytosolic components are required for proteasomal degradation of newly synthesized apolipoprotein B in permeabilized HepG2 cells. J Biol Chem 274, 17068–17074.
Sane AT, Seidman E, Peretti N, Kleme ML, Delvin E, Deslandres C, Garofalo C, Spahis S, Levy E (2017). Understanding chylomicron retention disease through Sar1b Gtpase gene disruption: insight from cell culture. Arterioscler Thromb Vasc Biol 37, 2243–2251.
Schilke BA, Ciesielski SJ, Ziegelhoffer T, Kamiya E, Tonelli M, Lee W, Cornilescu G, Hines JK, Markley JL, Craig EA (2017). Broadening the functionality of a J-protein/Hsp70 molecular chaperone system. PLoS Genet 13, e1007084.
Schmidt BZ, Watts RJ, Aridor M, Frizzell RA (2009). Cysteine string protein promotes proteasomal degradation of the cystic fibrosis transmembrane conductance regulator (CFTR) by increasing its interaction with the C terminus of Hsp70-interacting protein and promoting CFTR ubiquitylation. J Biol Chem 284, 4168–4178.
Segrest JP, Jones MK, De Loof H, Brouillette CG, Venkatachalapathi YV, Anantharamaiah GM (1992). The amphipathic helix in the exchangeable apolipoproteins: a review of secondary structure and function. J Lipid Res 33, 141–166.
Shevtsov M, Multhoff G, Mikhaylova E, Shibata A, Guzhova I, Margulis B (2019). Combination of anti-cancer drugs with molecular chaperone inhibitors. Int J Mol Sci 20. 10.3390/ijms20215284.
Siddiqi SA, Gorelick FS, Mahan JT, Mansbach CM 2nd (2003). COPII proteins are required for Golgi fusion but not for endoplasmic reticulum budding of the pre-chylomicron transport vesicle. J Cell Sci 116, 415–427.
Sikka P, Kapoor S, Bindra VK, Sharma M, Vishwakarma P, Saxena KK (2011). Statin intolerance: now a solved problem. J Postgrad Med 57, 321–328.
Sirwi A, Hussain MM (2018). Lipid transfer proteins in the assembly of apoB-containing lipoproteins. J Lipid Res 59, 1094–1102.
Smith LC, Pownall HJ, Gotto AM Jr (1978). The plasma lipoproteins: structure and metabolism. Annu Rev Biochem 47, 751–757.
Soti C, Nagy E, Giricz Z, Vigh L, Csermely P, Ferdinandy P (2005). Heat shock proteins as emerging therapeutic targets. Br J Pharmacol 146, 769–780.
Sparks JD, Zolfaghari R, Sparks CE, Smith HC, Fisher EA (1992). Impaired hepatic apolipoprotein B and E translation in streptozotocin diabetic rats. J Clin Invest 89, 1418–1430.
Stark JL, Mehla K, Chaika N, Acton TB, Xiao R, Singh PK, Montelione GT, Powers R (2014). Structure and function of human DnaJ homologue subfamily a member 1 (DNAJA1) and its relationship to pancreatic cancer. Biochemistry 53, 1360–1372.
Strickland E, Qu BH, Millen L, Thomas PJ (1997). The molecular chaperone Hsc70 assists the in vitro folding of the N-terminal nucleotide-binding domain of the cystic fibrosis transmembrane conductance regulator. J Biol Chem 272, 25421–25424.
Tatu U, Helenius A (1999). Interaction of newly synthesized apolipoprotein B with calnexin and calreticulin requires glucose trimming in the endoplasmic reticulum. Biosci Rep 19, 189–196.
Terada K, Mori M (2000). Human DnaJ homologs dj2 and dj3, and bag-1 are positive cochaperones of hsc70. J Biol Chem 275, 24728–24734.
Thiruvalluvan A, de Mattos EP, Brunsting JF, Bakels R, Serlidaki D, Barazzuol L, Conforti P, Fatima A, Koyuncu S, Cattaneo E, *et al*. (2020). DNAJB6, a key factor in neuronal sensitivity to amyloidogenesis. Mol Cell 78, 346–358.e349.
Tiwari S, Siddiqi SA (2012). Intracellular trafficking and secretion of VLDL. Arterioscler Thromb Vasc Biol 32, 1079–1086.
Veatch JR, McMurray MA, Nelson ZW, Gottschling DE (2009). Mitochondrial dysfunction leads to nuclear genome instability via an iron-sulfur cluster defect. Cell 137, 1247–1258.
Verma R, Chen S, Feldman R, Schieltz D, Yates J, Dohmen J, Deshaies RJ (2000). Proteasomal proteomics: identification of nucleotide-sensitive proteasome-interacting proteins by mass spectrometric analysis of affinity-purified proteasomes. Mol Biol Cell 11, 3425–3439.
Walker VE, Wong MJ, Atanasiu R, Hantouche C, Young JC, Shrier A (2010). Hsp40 chaperones promote degradation of the HERG potassium channel. J Biol Chem 285, 3319–3329.
Walsh P, Bursac D, Law YC, Cyr D, Lithgow T (2004). The J-protein family: modulating protein assembly, disassembly and translocation. EMBO Rep 5, 567–571.
Wang H, Chen X, Fisher EA (1993). N-3 fatty acids stimulate intracellular degradation of apoprotein B in rat hepatocytes. J Clin Invest 91, 1380–1389.
Ward NC, Watts GF, Eckel RH (2019). Response by Ward et al to letter regarding article, "Statin toxicity: mechanistic insights and clinical implications." Circ Res 124, e121–e122.
Welty FK (2020). Hypobetalipoproteinemia and abetalipoproteinemia: liver disease and cardiovascular disease. Curr Opin Lipidol 31, 49–55.
Wentink AS, Nillegoda NB, Feufel J, Ubartaite G, Schneider CP, De Los Rios P, Hennig J, Barducci A, Bukau B (2020). Molecular dissection of amyloid disaggregation by human HSP70. Nature 587, 483–488.
White AL, Graham DL, LeGros J, Pease RJ, Scott J (1992). Oleate-mediated stimulation of apolipoprotein B secretion from rat hepatoma cells. A function of the ability of apolipoprotein B to direct lipoprotein assembly and escape presecretory degradation. J Biol Chem 267, 15657–15664.
Wu X, Zhou M, Huang LS, Wetterau J, Ginsberg HN (1996). Demonstration of a physical interaction between microsomal triglyceride transfer protein and apolipoprotein B during the assembly of ApoB-containing lipoproteins. J Biol Chem 271, 10277–10281.
Xu D, Tong X, Sun L, Li H, Jones RD, Liao J, Yang GY (2019). Inhibition of mutant Kras and p53-driven pancreatic carcinogenesis by atorvastatin: Mainly via targeting of the farnesylated DNAJA1 in chaperoning mutant p53. Mol Carcinog 58, 2052–2064.
Yeung SJ, Chen SH, Chan L (1996). Ubiquitin-proteasome pathway mediates intracellular degradation of apolipoprotein B. Biochemistry 35, 13843–13848.
Yokota S, Kitahara M, Nagata K (2000). Benzylidene lactam compound, KNK437, a novel inhibitor of acquisition of thermotolerance and heat shock protein induction in human colon carcinoma cells. Cancer Res 60, 2942–2948.
Yu HY, Ziegelhoffer T, Craig EA (2015a). Functionality of Class A and Class B J-protein co-chaperones with Hsp70. FEBS Lett 589, 2825–2830.
Yu HY, Ziegelhoffer T, Osipiuk J, Ciesielski SJ, Baranowski M, Zhou M, Joachimiak A, Craig EA (2015b). Roles of intramolecular and intermolecular interactions in functional regulation of the Hsp70 J-protein co-chaperone Sis1. J Mol Biol 427, 1632–1643.
Zhang H, Peters KW, Sun F, Marino CR, Lang J, Burgoyne RD, Frizzell RA (2002). Cysteine string protein interacts with and modulates the maturation of the cystic fibrosis transmembrane conductance regulator. J Biol Chem 277, 28948–28958.
Zhang Y, Nijbroek G, Sullivan ML, McCracken AA, Watkins SC, Michaelis S, Brodsky JL (2001). Hsp70 molecular chaperone facilitates endoplasmic reticulum-associated protein degradation of cystic fibrosis transmembrane conductance regulator in yeast. Mol Biol Cell 12, 1303–1314.
Zhou M, Fisher EA, Ginsberg HN (1998). Regulated Co-translational ubiquitination of apolipoprotein B100. A new paradigm for proteasomal degradation of a secretory protein. J Biol Chem 273, 24649–24653.
Zhou M, Wu X, Huang LS, Ginsberg HN (1995). Apoprotein B100, an inefficiently translocated secretory protein, is bound to the cytosolic chaperone, heat shock protein 70. J Biol Chem 270, 25220–25224.
Zimmermann TS, Lee AC, Akinc A, Bramlage B, Bumcrot D, Fedoruk MN, Harborth J, Heyes JA, Jeffs LB, John M, *et al.* (2006). RNAi-mediated gene silencing in non-human primates. Nature 441, 111–114.